

# Sulfur cycling in the aftermath of a 635-Ma snowball glaciation: Evidence for a syn-glacial sulfidic deep ocean

Matthew T. Hurtgen<sup>a,1</sup> Galen P. Halverson<sup>b</sup>  
Michael A. Arthur<sup>c</sup> Paul F. Hoffman<sup>d</sup>

<sup>a</sup>*Department of Geological Sciences, Northwestern University, Evanston, IL 60208 USA*

<sup>b</sup>*UMR 5563, Laboratoire des Mécanismes et Transferts en Géologie (LMTG), Université Paul Sabatier, 14 avenue Edouard Belin, 31400 Toulouse, France*

<sup>c</sup>*Penn State Astrobiology Research Center and Department of Geosciences, Pennsylvania State University, University Park, Pennsylvania 16802 USA*

<sup>d</sup>*Dept. of Earth and Planetary Sciences, Harvard University, Cambridge, MA 02138 USA*

---

## Abstract

We have analyzed  $\delta^{34}\text{S}$  (sulfate and pyrite),  $\delta^{18}\text{O}_{\text{carbonate}}$  and  $\delta^{13}\text{C}_{\text{carbonate}}$ , and major and trace elemental concentrations, including extractable Fe and Mn phases, in four sections of the Maieberg Formation, the cap carbonate sequence to the Marinoan glaciation in northern Namibia.  $\delta^{34}\text{S}_{\text{sulfate}}$  profiles and other geochemical characteristics in the basal, transgressive cap dolostone (Keilberg Member) are nearly identical in all sections and indicate deposition from a water mass with very low sulfate concentrations. In the overlying interval that consists of rhythmites deposited during the transgressive high-stand, large geochemical disparities occur between sections that we interpret to have been deposited in open-ocean versus restricted settings. In the former, a large negative shift in  $\delta^{34}\text{S}_{\text{sulfate}}$  of  $\sim 20\%$  above the cap dolostone accompanies a change in mineralogy from dolomite to limestone, a sharp decrease in  $\delta^{18}\text{O}$  and  $\delta^{13}\text{C}$ , and a positive spike in Fe and Mn concentrations. In the latter, dolomite persists above the cap dolostone,  $\delta^{34}\text{S}_{\text{sulfate}}$  increases abruptly,  $\delta^{18}\text{O}$  and  $\delta^{13}\text{C}$  are invariant, and a spike in Mn and Fe concentrations is present, but subtle. These contrasting geochemical signatures in coeval sections can be explained by strong lateral chemical gradients that developed as cold, euxinic deep water and a cap of warm, oxic, brackish water flooded the continental shelf during the post-glacial transgression. The geochemical differences between open-ocean and restricted sections diminishes upsection, presumably recording the gradual mixing and homogenization of the waters along the Otavi platform.

*Key words:* sulfur isotopes, carbon isotopes, cap carbonate, Neoproterozoic,

## 1 Introduction

At least twice during the Neoproterozoic (1000 – 542 Ma), continental glaciers reached sea level in the low latitudes [1–4]. Geologic evidence [5, 6] suggests that the entire ocean froze over during these glaciations due to ice-albedo feedback [7–9]. According to the snowball hypothesis [5, 6, 10], such a glaciation would have endured millions of years, until sufficient volcanically-derived CO<sub>2</sub> [ $>0.2$  bar; 11] accumulated in the atmosphere to counteract the extremely potent climate stabilizing effect of a high-albedo, frozen earth. The combined effect of the extraordinarily high pCO<sub>2</sub>, the ice-albedo feedback, and increased water vapor in the atmosphere would have driven a rapid transition from ice-house to extreme greenhouse once the frozen earth began to thaw [6, 12]. This aftermath is recorded in the form of sedimentologically and geochemically distinctive cap carbonate sequences that drape Neoproterozoic glacial deposits worldwide [e.g., 6, 12–17].

Due to its excellent exposure in a range of paleogeographic settings, high carbonate-content [18, 19], and rapid rate of deposition [20], the 635 Ma [20, 21] Maieberg Formation cap-carbonate sequence in northern Namibia is ideally suited for reconstructing the chemistry of the post-Marinoan ocean. Detailed  $\delta^{13}\text{C}$  data on the Maieberg Formation have been published previously [6, 19]. In this paper we contribute complementary  $\delta^{13}\text{C}$  and  $\delta^{18}\text{O}$  data from the Maieberg Formation, along with new results on the  $\delta^{34}\text{S}$  composition of carbonate-associated sulfate (CAS), pyrite, and Fe and Mn concentrations from acid soluble (carbonate bound) and dithionite-extractable (oxides and oxyhydroxides) phases. These data corroborate previous results from the Maieberg Formation and other correlative cap carbonates that exhibit large and rapid shifts in the  $\delta^{34}\text{S}$  composition of both CAS [22, 23] and pyrite [24, 25] following the Marinoan glaciation, but also reveal spatial geochemical gradients during the high-stand systems tract, between sections deposited in open-ocean versus restricted settings. The geochemical signatures preserved within the Maieberg Formation can be explained by the development of a very stably stratified ocean in the aftermath of glaciation, in which a surface mixed layer of brackish and oxic water, dominated by surface run-off, caps cold, anoxic deep waters, resulting in a large surface-to-deep redox gradient. We attribute the  $\delta^{34}\text{S}_{sulfate}$  difference of up to  $\sim 20\%$  in the middle Maieberg Formation to strong lateral chemical gradients that developed along a pale-

---

<sup>1</sup> Corresponding author: matt@earth.northwestern.edu

oenvironmental offshore-onshore transect as the redox chemocline transgressed the Otavi Platform.

## 2 Background

### 2.1 *The Neoproterozoic Sulfur Cycle*

In the modern ocean, the concentration of sulfate is 28 mM and the residence time is 10 to 20 Myr [26]. Because of its relatively high concentration and long residence time, the sulfur-isotope composition of this sulfate ( $\delta^{34}\text{S}_{\text{sulfate}}$ ), which today is 21‰ [27], is both homogenous throughout the ocean basins, and buffered against short-term (< 1 Myr.) variations. The  $\delta^{34}\text{S}$  composition of seawater sulfate in steady state is a function of the mass and isotopic composition of the sulfur fluxes into and out of the ocean. Sulfate is delivered to the oceans mainly through the oxidative weathering of  $^{34}\text{S}$ -depleted pyrite and other sulfides and the dissolution of evaporite minerals. It is removed from the ocean mainly as pyrite, following bacterial sulfate reduction, which entails a large isotopic fractionation [28, and references therein], and the precipitation of evaporite minerals, which incurs negligible fractionation [29]. Assuming the isotopic composition of sulfur input to the ocean to be roughly constant, the main controls on marine  $\delta^{34}\text{S}$  of the oceans over geological time scales is the net fractionation between seawater sulfate and pyrite buried in sediments ( $\Delta^{34}\text{S}$ ) and the fraction of total sulfur buried as pyrite [ $f_{\text{pyrite}}$ ; 26].  $\delta^{34}\text{S}_{\text{sulfate}}$  has changed by about 0.8‰ since the beginning of the Pleistocene and has varied between 17.5 and 22.5‰ during the Cenozoic [30].

Although average  $\delta^{34}\text{S}_{\text{sulfate}}$  of the Neoproterozoic ocean appears to be similar to that of the Cenozoic [22, 31], average  $\Delta^{34}\text{S}$  values were lower and  $f_{\text{pyrite}}$  higher [31, and references therein]. Furthermore, variations in  $\delta^{34}\text{S}_{\text{sulfate}}$ , as recorded in carbonate-associated sulfate (CAS), were much greater in magnitude [22, 23]. Although marine sulfate concentrations are poorly quantified for this time period [32], the high amplitude variability in  $\delta^{34}\text{S}_{\text{sulfate}}$ , coupled with low CAS concentrations (relative to Cenozoic carbonates), suggests that Neoproterozoic oceanic sulfate concentrations were on average much lower than modern values—perhaps 10% [e.g., ca. 3 mM; 22, 23]. Because sulfate concentrations were likely significantly lower in the Neoproterozoic, the sulfate reservoir would have been more susceptible to the development of isotopic heterogeneities. The nearly quantitative removal of sulfate from the oceans predicted to occur during snowball events [22] would have rendered the post-glacial oceans particularly prone to large variations and isotopic heterogeneities. Previous work on cap carbonate sequences in Namibia and Death Valley has shown variations of 17 to 30‰ over narrow stratigraphic ranges and

values as high as 40‰ [22, 23]. Making sense of these variations and the general response of the sulfur cycle should reveal important information on the behavior of the oceans during the aftermath of Neoproterozoic glaciation.

## *2.2 Post-Marinoan cap-carbonate sequences*

Neoproterozoic cap carbonate sequences overlie glacial deposits and correlative sequence boundaries of the ca. 710 Ma Sturtian [33, 34] and ca. 635 Ma Marinoan [21] glaciations. Although the cap carbonates to each glacial event are distinct one from the other [19, 35], both stand out amidst the background stratigraphy as comprising unusually thick sequences [6]. The Marinoan cap carbonate sequences are the more complete and include at the base a laterally extensive transgressive cap dolostone, which in platform settings is commonly 5 - 20 m thick. Typical cap dolostones contain inversely graded layers of macropeloids, low-angle cross-stratification, and giant wave ripple structures [e.g., 10, 17, 36]. A flooding surface at the top of the cap dolostone coincides with an abrupt shift to either limestone or shale. In some cases, most notably in shelf margin sections of the Hayhook Formation in the Mackenzie Mountains (NW Canada), seafloor barite cements occur at this contact [12]. The layer of sea-floor barite at the top of the Ravensthorpe cap dolostone is continuous for >150 km parallel and >30 km perpendicular to the shelf edge. The occurrence of sedimentary barite at this stratigraphic level provides a key constraint on the evolution of the post-Marinoan ocean since the very low solubility of barite indicates that it formed from the mixing of two distinct water masses. Given the link of the barite precipitation with transgression, which was driven by the melting of the Marinoan glaciers, then it seems likely that these two water masses were the cold, deep ocean, relict from the snowball, and an oxic, buoyant surface layer dominated by continental run-off.

The barite is associated with the more widespread, but not extensive, formerly aragonitic seafloor cements [12], which are locally well developed in the Hayhook Formation of northwest Canada and in the Maieberg Formation in Namibia, where they coalesce to form patch reefs. The “crystal fan” reefs were flooded and smothered by background micrite or clastic sedimentation [17] at the level of maximum flooding in the cap-carbonate sequence. The remainder of the cap-carbonate sequence consists of an upward-shoaling stack of sediments, culminating in an exposure surface typically several hundreds of meters above the base of the sequence. Carbonate content decreases precipitously above the cap dolostone in many Marinoan cap-carbonate sequences [12, 19], such as in the siliciclastic-dominated successions in South Australia [16] and northeastern Norway [37], where the cap dolostone is overlain by hundreds of meters of purple and red shale and siltstone. The Maieberg Formation is an exception, and carbonate continues throughout the Tsumeb Subgroup

(see below).

The cap-carbonate sequences are well known for recording a large negative  $\delta^{13}\text{C}$  anomaly, the origin of which is typically linked to the glaciation with which they are temporally associated [6, 16, 35, 38, 39]. The  $\delta^{13}\text{C}$  trends through the Marinoan cap dolostones are impressively similar worldwide, displaying average  $\delta^{13}\text{C}$  values of  $-3$  to  $-4\text{‰}$ , and a slightly negative trend upsection [19]. Where limestone occurs above the cap dolostone,  $\delta^{13}\text{C}$  values shift negative by 1 to 2‰ at the dolomite-limestone transition [e.g., 16, 40, 41].  $\delta^{18}\text{O}$  values, though generally more variable, also shift downward by 3 to 6‰ at this transition [e.g., 16]. Variation of 2-3‰ in  $\delta^{13}\text{C}$  values between inner and outer shelf sections has been reported from the coeval [20] lower Doushantuo Formation in south China and interpreted as evidence for stratified oceans following the Marinoan glaciation [42, 43].

### 2.3 *The Otavi Group*

The Otavi Group lies on the southwestern margin of the Congo craton where it is well exposed in the Kaoko and central Damara fold-and-thrust belts in northwestern and north-central Namibia (Fig. 1). It is disconformably underlain by fluvial clastics of the Nosib Group and paraconformably overlain by foreland basin siliciclastics of the Mulden Group, deposited following the ca. 580 Ma [45] collision between the western margin of the Angola block [which now comprises the southwestern Congo craton but might have been separate until the late Neoproterozoic; 46] and the Paraná block of southeastern Brazil [47, and references therein]. The Otavi Group (Fig. 1b,c) comprises the Ombombo, Ugab, Abenab, and Tsumeb subgroups, the latter two of which are floored by the glaciogenic Chuos (Sturtian) and Ghaub (Marinoan) formations [48]. Neoproterozoic successions of equivalent age also occur in central (Witvlei Group) and southwest (Gariiep Group) Namibia [49].

During Otavi Group deposition, the Otavi carbonate platform in the north of the depositional basin (Fig. 1) was progressively differentiated from the deep-water Outjo basin to the south [50] as a result of north-south crustal stretching [51]. The mixed siliclastic-carbonate Ombombo Subgroup occurs only on the northern platform, where it was tilted on a Paleoproterozoic basement high [52] to the south and beveled beneath the Sturtian glacials [18]. A  $760\pm 1$  Ma U-Pb age on an ash bed in the middle Ombombo Subgroup; [Fig. 1; 19] is significantly older than the base of the Ugab Subgroup, which lies beneath the Chuos Formation on the southern margin of the craton [21] and is constrained to be younger than  $746\pm 2$  Ma [44] by an U-Pb age on the underlying Naauwpoort Volcanics (Fig. 1). The Chuos Formation is highly variable in thickness, heterolithic, and, typical of (but not unique to) Sturtian

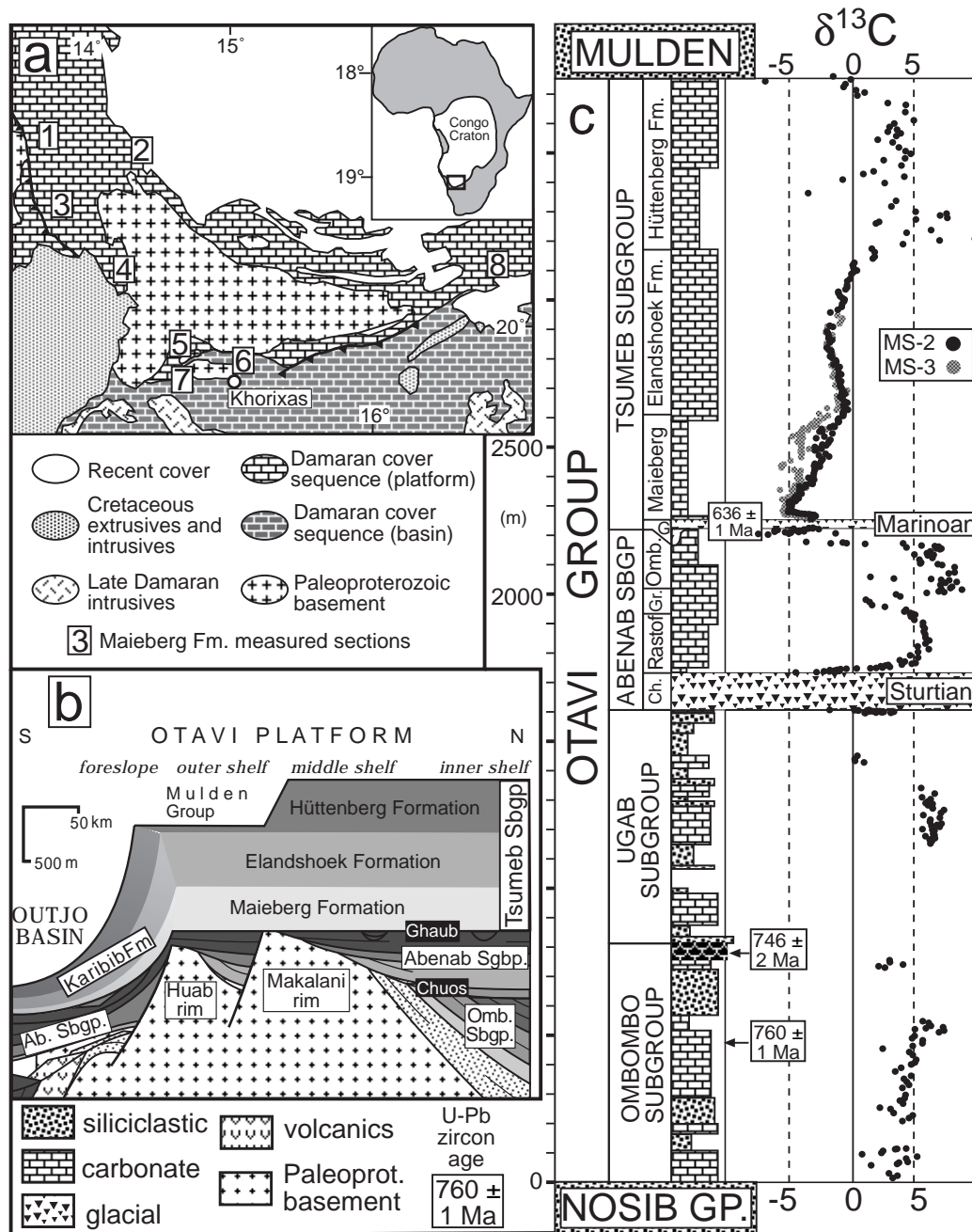


Fig. 1. a. Simplified geological map showing the distribution of the Otavi Group in northwestern and north-central Namibia, and the location of measured sections used in this study. Inset map shows location of the study area on the southwestern tip of the Congo craton (Angola block) on the African continent. b. Schematic north-south stratigraphic cross-section of the Otavi Group [modified from 19], showing the location of prominent paleotopographic basement highs and the segmentation of the Otavi basin into the deepwater Outjo basin in the south and the Otavi platform in the north. c. Composite stratigraphic and  $\delta^{13}\text{C}$  profiles through the Otavi Group on the northern platform, modified from Halverson et al. [19], and based on the assumption (see text) that the Ugab Subgroup in the Outjo basin is entirely younger than the Ombombo Subgroup and absent on the Otavi Platform.  $\delta^{13}\text{C}$  for the Tsumeb Subgroup is from two measured sections (MS2,3). U-Pb zircon ages, from youngest to oldest, are from [19, 21, 44]. The legend in the lower left hand corner is for Fig. 1b and 1c. Abbreviations: Ch = Chuos Formation, Gr = Grais Formation, Omb. = Ombombo Formation, G. = Ghaub Formation.

glacial deposits, contains banded iron-formation (BIF) and is overlain by a cap carbonate sequence (Rasthof Fm.) with a negative  $\delta^{13}\text{C}$  anomaly [53](Fig. 1).

Extension continued along the southern margin of the Angola block through Abenab times, uplifting at least two basement blocks (Makalani and Huab rims) and bisecting the Otavi platform (Fig. 1). Carbon-isotopic data from the Abenab Subgroup suggest increased restriction from the outer shelf in the south to the inner shelf on the northern Otavi platform [19]. The base of the Ombaatjie Formation approximates the onset of the Otavi passive margin [53]. In the upper Ombaatjie Formation,  $\delta^{13}\text{C}$  values drop from +8‰ to -5‰ through 20 - 40 m of unremarkable dolomite section, heralding the onset of the Ghaub glaciation [53]. A decrease in  $\Delta^{34}\text{S}$  coincides with the negative  $\delta^{13}\text{C}$  anomaly and implies a major perturbation in the sulfur cycle [31] accompanied a change in the carbon cycle. The upper Ombaatjie Formation is variably truncated beneath the Ghaub Formation, which consists predominantly of carbonate matrix diamictite, with clasts derived almost exclusively from the underlying Abenab Subgroup. The Ghaub Formation is patchy and thin throughout most of the Otavi platform, but is continuous and 40 - 80 m thick on the continental foreslope (Fransfontein Ridge), where it has been interpreted to represent a single glacial advance and retreat cycle [54]. Hoffmann et al. [21] obtained a U-Pb date of  $635.5 \pm 1.2$  Ma from an ash bed in the upper Ghaub Formation in central Namibia (central zone of the Damara belt), providing the first direct age on the Marinoan glaciation.

### 2.3.1 The Maieberg Formation

The Ghaub glacials are at the base of the Tsumeb Subgroup, a thick package of carbonates (<3000 m) that comprises most of the passive margin sequence in northern Namibia. The top of the Tsumeb Subgroup is a major erosional paraconformity beneath the Mulden Group, which in places has removed the Otavi Group entirely [55]. The Maieberg Formation is the cap carbonate to the (Marinoan) Ghaub glacials and is comprised of a  $\sim$  250 - 400 m thick transgressive-high stand sequence that filled accommodation space generated during the long-lived Marinoan glaciation [6, 18]. A pair of precise U-Pb zircon ages from ashes in the equivalent lower Doushantuo Formation of South China [20], indicate that the entire Maieberg Formation was deposited in <3 Ma. The Maieberg Formation, defined by Hoffman and Halverson [50] to include the entire cap carbonate sequence, bound above by a mappable sequence boundary, is divided here into three members: the basal (formally defined) *Keilberg Member* (cap dolostone), a *middle member* comprising limestone and dolomite rhythmite, and an *upper member* consisting of dolomite grainstone.

The distinctive Keilberg Member cap dolostone is the transgressive base of the

cap sequence and is ubiquitous on the Otavi platform. On the northern platform, the Keilberg Member is 10 - 25 m thick, but it is significantly thicker (50 - 75 m) on the rims of the Makalani and Huab topographic highs in the southern part of the basin [Fig. 2, 56]. The Keilberg Member contains a series of unusual sedimentary structures, typical of other Marinoan cap dolostones [12], deposited during the post-glacial transgression, including microbial bioherms and associated tubular and sheet infillings [“tubes”, cf. 57] and megaripple structures towards the top [58], interpreted to record deposition at depths between 200 and 400 m under oscillatory flow, achieved by sustained, intense winds that were initiated by high atmospheric pressure gradients in the aftermath of glaciation [10].

The Keilberg Member is everywhere bound above by a marine flooding surface without hiatus [12], and in typical platform settings [measured section (MS) 2,3,5,8; Fig. 3] is overlain by recessive, marly limestone rhythmites with thin interbeds of allodapic dolomite forming the base of the middle member. Above a maximum flooding surface in this lower interval, the middle member grades into nearly pure pink limestone then gray dolomite rhythmite. Large-scale swaley cross-stratification is common in the upper part of the middle member. The contact between the middle and upper members is transitional, with the gray dolomite rhythmites grading into gray, coarsening-upward, cross-bedded grainstone. The top of the Maieberg Formation is a heavily silicified exposure surface. The overlying Elandshoek and Hüttenberg formations comprise cyclic parasequences of predominantly cherty, dolomite grainstone.

Although the sequence of facies in the Maieberg Formation is the same throughout the platform, the middle member is not always limestone (Fig. 2). In one section in the Otavi Mountainland, near the type section, the Keilberg Member is instead overlain by shale and is nearly devoid of carbonate, presumably due to the proximity of this section to a major source of siliciclastic sediments into the basin. Elsewhere, and of significance to this study, dolomite persists above the cap dolostone. We present two all-dolomite Maieberg sections here: MS-1 (Figs. 2, 6) is our northernmost section, and MS-4 (Figs. 2, 5) is located on the Makalani rim (Figs. 1,2), where the Maieberg Formation onlaps a basement high [59]. Stratigraphic geometries indicate that the Makalani rim (MS-4) was deposited in a relatively shallow part of the Otavi platform, and it stands to reason that this and other shallow platform environments furnished the fine dolomite turbidites found in the lower part of the middle member in deeper water sections. The paleogeographic setting of the northern section (MS-1) is less certain, but its location far to the north of the shelf margin suggests that it occupied a relatively restricted environment. Moreover, the two all-dolomite sections are thinner overall than adjacent limestone-bearing sections, implying lower subsidence rates.

The Karibib Formation is the condensed, slope-facies equivalent of the Tsumeb

Subgroup in the Outjo basin [Fig. 2; 21, 60] and typically consists of rhythmites, fine turbidites, and grain and debris flow deposits. Near the shelf break, the Karibib Formation includes a middle interval of limestone, but more distal sections are entirely dolomite (Fig. 2). In sections near the shelf margin, the Karibib Formation shoals upward into high energy grainstone and domal stromatolite facies, manifesting the southward progradation of the Tsumeb carbonate platform [56]. The Keilberg Member is absent in the Karibib Formation, but sheet-crack cements occur  $\sim 1$  m above the top of the Ghaub Formation [58] and are reminiscent of some other Marinoan cap dolostones [61].

In most sections, the upper Keilberg Member is accompanied by a negative shift in  $\delta^{13}\text{C}$  and  $\delta^{18}\text{O}$  compositions (Figs. 3, 4).  $\delta^{13}\text{C}$  reaches a low of  $-5.5\%$  in the middle member at approximately the level of the maximum flooding surface, above which it gradually rises, approaching  $0\%$  near the top of the formation [6, 50]. The Karibib Formation preserves a similar but condensed  $\delta^{13}\text{C}$  anomaly that has been reproduced in multiple sections [6, 19, 50]. The Maieberg isotope anomaly occupies 300-400 m of strata on the platform, 40 m on the medial foreslope (Fransfontein), and 25 m on the distal foreslope (Bethanis).

### 3 Methods

#### 3.1 Sulfur Isotopes

Sulfur isotope ratios are expressed as per mil ( $\%$ ) deviations from the S isotope composition of Cañon Diablo Troilite (CDT) using the conventional delta ( $\delta^{34}\text{S}$ ) notation. All new sulfur isotope data and accompanying elemental data are presented in tabulated form in Supplementary Tables 1-4.

The method used here for extracting carbonate-associated sulfate (CAS) from carbonate rocks is modified slightly from that described by Burdett et al. [62]. Carbonate rock samples were first cut to remove weathered surfaces and veins, then pulverized. An aliquot of 15 to 80 g of sample powder was then soaked in a 5.25% sodium hypochlorite solution for  $\sim 24$  hours. The sediment was rinsed with deionized water, dissolved in 3 N HCl, and the insoluble residue was removed using  $0.5\ \mu\text{m}$  filters. Approximately 25-30 mL of saturated  $\text{BaCl}_2$  was added to the filtrate. Precipitated  $\text{BaSO}_4$  (barite) was filtered through Whatman No. 42 ashless filter papers.

Approximately 2 to 10 mg of  $\text{BaSO}_4$  barite was mixed with  $\text{V}_2\text{O}_5$  and combusted in an Elemental Analyzer at  $1000^\circ\text{C}$ .  $\text{SO}_2$  was isolated cryogenically

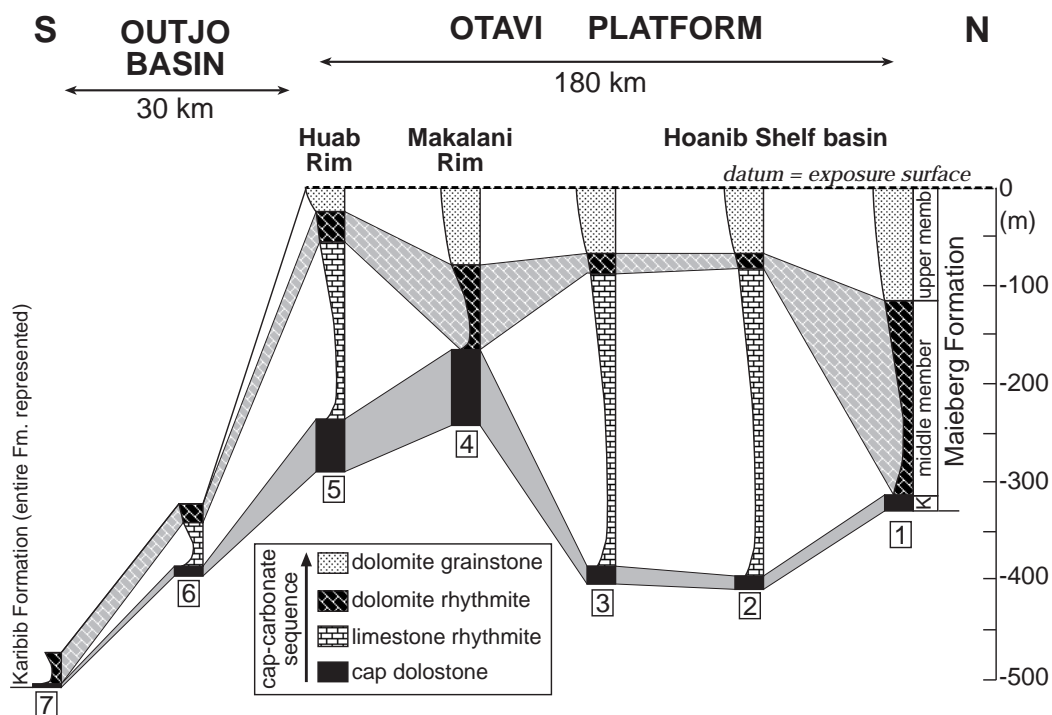


Fig. 2. Selected stratigraphic columns of the Maieberg Formation showing a paleogeographic cross-section from the northern Otavi platform to the Outjo basin in the south [53]. Note that in the inferred deepest (basin) and shallowest (Makalani Rim and proximal sections) environments, the Maieberg Formation is entirely dolomite. Each stratigraphic column is keyed to Fig. 1. Measured-Section 8, is located ca. 200 km to the east of this north-south cross-section, but occupies a paleogeographic position similar to MS-5—near the shelf margin. K = Keilberg Member.

on a vacuum line and total S mass was determined. The purified  $\text{SO}_2$  was sealed in pyrex tubing and analyzed on a VG Prism Series II isotope ratio mass spectrometer. Sulfur isotope results were generally reproducible within  $\pm 0.2\%$ , based on repeat analysis of standards.

Pyrite was extracted from the insoluble residue using the chromium reduction method [63], which liberates  $\text{H}_2\text{S}$  from specific reduced inorganic forms of sulfur (pyrite sulfur, acid-volatile sulfur, and elemental sulfur). The  $\text{H}_2\text{S}$  was then precipitated as  $\text{Ag}_2\text{S}$ , aliquots of which were combusted in the presence of cupric oxide for a quantitative conversion to  $\text{SO}_2$ . The sulfur-isotopic composition of the  $\text{SO}_2$  was analyzed via the same method described above.

### 3.2 Carbon and oxygen isotopes

Carbon and oxygen isotope ratios presented in this paper are expressed in ‰ deviations relative to VPDB in the standard delta ( $\delta^{13}\text{C}$ ,  $\delta^{18}\text{O}$ ) notation. New data presented in this paper are presented in tabulated form in Supplementary Tables 1-4. All data were acquired on an Optima dual inlet IRMS at the Harvard University Laboratory for Geochemical Oceanography. Average external precision is estimated to be better than 0.1‰ for both carbon and oxygen, based on repeat analyses of standards. Analytical methods are described in greater detail in Halverson et al. [36].

### 3.3 Elemental Chemistry

Concentrations of Ca, Mg, Fe, Mn, Sr and Ba were determined on an inductively coupled plasma (ICP) spectrophotometer in the Penn State Materials Characterization Laboratory. Approximately 0.25 mg of sample was weighed, reacted with 5% acetic acid and diluted with deionized water. Insoluble residues were removed via filtration, dried and weighed. The mass of insoluble residue was subtracted from the original mass to calculate trace and minor-element concentrations relative to 100% carbonate and reported in ppm. Tabulated data are presented in Supplementary Tables 1-4. Duplicate extractions using unknowns yielded standard deviations of less than 10% of the mean.

### 3.4 Buffered Fe and Mn extractions

Fe extractions using buffered dithionite (sodium dithionite in a pH 4.8 buffer comprising 0.35 M acetic acid and 0.2 M sodium citrate; room temperature) were performed [64]. The phases extracted via this method are dominated by iron oxides and oxyhydroxides as opposed to the acid-soluble fraction that is comprised of mainly  $\text{Fe}^{2+}$  ( $\text{Fe}_{carb}$ ) and  $\text{Mn}^{2+}$  ( $\text{Mn}_{carb}$ ) that substituted into carbonate minerals. Iron bound in sulfide minerals was not quantified. Dithionite-soluble iron ( $\text{Fe}_{ox}$ ) and manganese ( $\text{Mn}_{ox}$ ) concentrations were measured by ICP spectrophotometry as described above. Tabulated data are presented in Supplementary Tables 1-4.

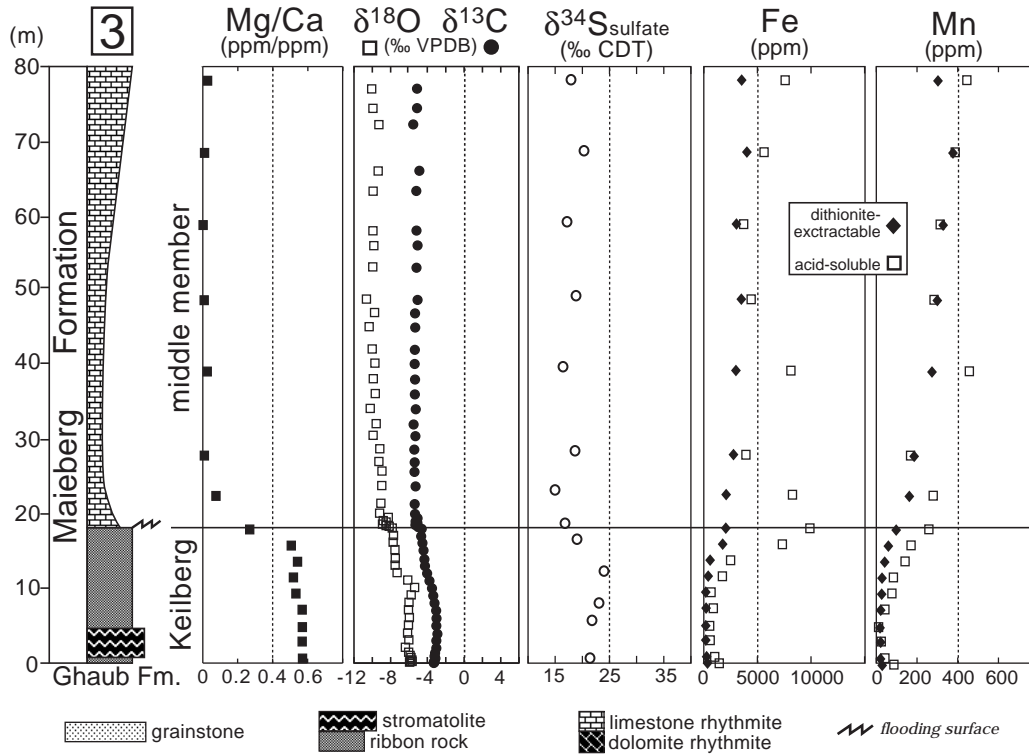


Fig. 3. Stratigraphic column and geochemical data for Measured Section 3. Refer to Figure 1 for a complete stratigraphic and  $\delta^{13}\text{C}$  profile for the Maieberg Formation in this location. Refer to the legend for Figs. 3 - 6. See Supplementary Table 1 for tabulated data.

## 4 Results

Here we present stratigraphic and geochemical data from four measured sections of the Maieberg Formation from the Otavi platform, representing what we interpret to be two contrasting depositional environments: restricted versus open marine. These four sections are a subset of a much larger collection of stratigraphic sections and accompanying  $\delta^{13}\text{C}$  and  $\delta^{18}\text{O}$  data, much of which has been presented separately [12, 18, 19, 50].

### 4.1 Measured section 3

Measured section 3, located in the Khowarib Schlucht in the center of the northern platform (Fig. 1), is a characteristic section of the Maieberg Formation. Detailed  $\delta^{34}\text{S}$  and elemental data have been acquired on only the lowermost 80 m of the section (Fig. 3); however, the complete stratigraphic and carbon isotopic profile from this section are included in the composite section of the Otavi Group presented in Figure 1. The Keilberg Member and

the contact with the underlying Ghaub Formation (and Ombaatjie Formation where the Ghaub is absent) are particularly well exposed.

The  $\delta^{13}\text{C}$  data in the lower Maieberg Formation at MS-3 define a very smooth profile (Fig. 3).  $\delta^{13}\text{C}$  compositions average  $\sim -3\text{‰}$  through the Keilberg Member and decrease slightly toward the top of the cap dolostone, followed by a more abrupt drop associated with the shift from dolomite to limestone.  $\delta^{13}\text{C}$  compositions continue to decline to a low of  $\sim -5.5\text{‰}$  in the lower middle member.  $\delta^{18}\text{O}$  compositions are slightly more variable, but otherwise parallel the  $\delta^{13}\text{C}$  profile with a similar negative shift concurrent with the dolomite-limestone transition. Although the sulfur isotope data are not nearly as detailed, they do show a smooth rise in  $\delta^{34}\text{S}_{\text{sulfate}}$  from 16 to 24‰ within the Keilberg Member, followed by a drop of over 10‰ spanning the dolomite-limestone transition.  $\delta^{34}\text{S}_{\text{sulfate}}$  remains low (15 - 20‰) throughout the 60 m of sampled middle member.

Both acid-soluble iron ( $\text{Fe}_{\text{carb}}$ ) and dithionite-soluble iron ( $\text{Fe}_{\text{ox}}$ ) concentrations remain relatively low through the lower half of the cap dolostone, but begin to rise towards the top (Fig. 3).  $\text{Fe}_{\text{carb}}$  spikes to a high of 10,000 ppm precisely at the top of the cap dolostone and remains high in the overlying limestone, whereas the rise in  $\text{Fe}_{\text{ox}}$  is more subtle and does not peak at this boundary. Changes in  $\text{Mn}_{\text{carb}}$  and  $\text{Mn}_{\text{ox}}$  concentrations are similar to those in iron, although concentrations are much lower (450 ppm), and the peak in  $\text{Mn}_{\text{carb}}$  occurs 20 m above the dolomite-limestone transition.

#### 4.2 Measured section 8

Measured section 8 (Fig. 4) is our easternmost section and is located on Arbeitsgenot Farm,  $\sim 80$  km to the west of the type section of the Maieberg Formation in the Otavi Mountainland. Both the Ombaatjie Formation (109 m) and the Maieberg Formation ( $\sim 220$  m) are relatively thin in this section, but are stratigraphically homologous to sections on the southern margin (Huab Rim) of the northern platform and likely were deposited in a similar, shelf margin environment.

$\delta^{13}\text{C}$  and  $\delta^{18}\text{O}$  show virtually the same pattern in the Keilberg Member here as in MS-3, with the exception that the negative offset across the dolomite-limestone transition is more pronounced. The  $\delta^{34}\text{S}_{\text{sulfate}}$  profile in the Keilberg Member is also similar, with a rise of  $>10\text{‰}$ , followed by a decline of nearly 20‰ spanning the top of the Keilberg member and the base of the middle member.  $\delta^{34}\text{S}_{\text{sulfate}}$  is relatively stable through most of the middle member, but begins to increase just below the switch from limestone to dolomite.  $\delta^{34}\text{S}_{\text{sulfate}}$  then levels off near 40‰ in the upper member. Limited  $\delta^{34}\text{S}$  data from finely

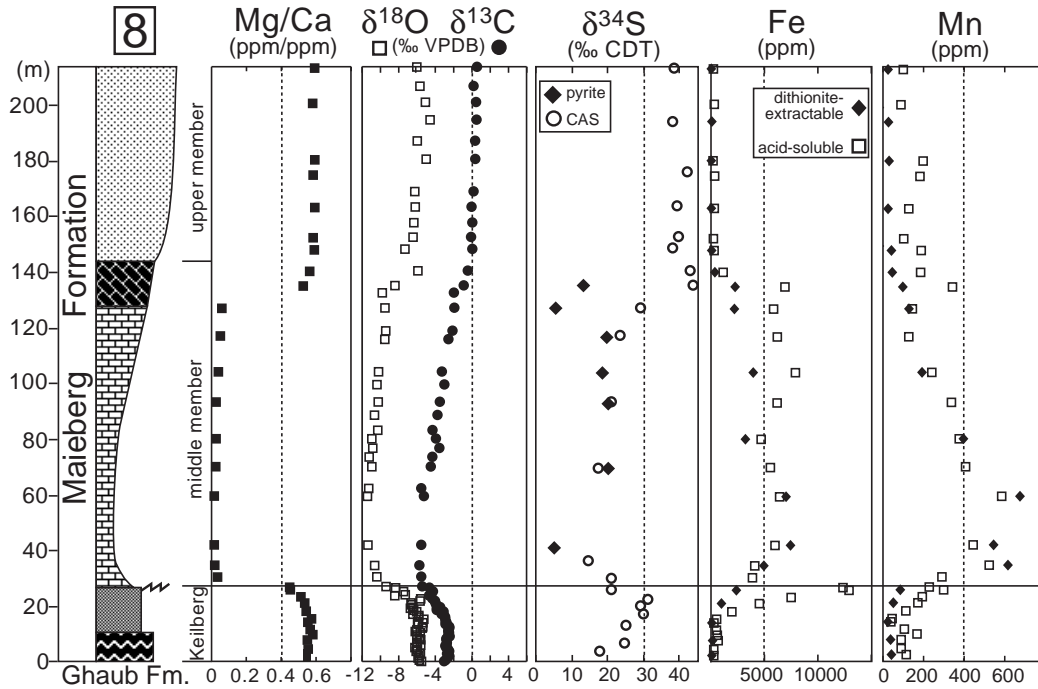


Fig. 4. Stratigraphic column and geochemical data for Measured Section 8, which is located far to the east of the N-S cross-section shown in Figure 2, but was deposited near the shelf edge, similar to MS-5. Refer to Figure 3 for legend, and see Supplementary Table 2 for tabulated data.

disseminated pyrite in the same samples are nearly identical to  $\delta^{34}\text{S}_{\text{sulfate}}$  through most of the limestone interval, but  $\delta^{34}\text{S}_{\text{pyrite}}$  begins to decrease in step with the increase in  $\delta^{34}\text{S}_{\text{sulfate}}$  near the top of the middle member.

Similar to MS-3, iron concentrations begin to increase in the upper Keilberg Member. Whereas  $\text{Fe}_{\text{carb}}$  concentration spikes to  $\sim 13,000$  ppm precisely at the dolomite–limestone boundary, before declining sharply in the lower part of the middle member,  $\text{Fe}_{\text{ox}}$  concentrations continue to increase across this contact, reaching a high of  $\sim 7,000$  ppm near the level of maximum flooding (Fig. 4). Changes in Mn concentration again roughly mirror those of Fe, with peak concentrations of both  $\text{Mn}_{\text{carb}}$  and  $\text{Mn}_{\text{ox}}$  ( $\sim 600$  ppm) occurring at the base of the middle member. Both Fe and Mn concentrations decrease upsection to levels approximately equal to those in the lower half of the cap dolostone.

#### 4.3 Measured section 4

Measured section 4 (Fig. 5) is located southwest of MS-3, on the eastern limb of the Grootberg Syncline to the northwest of Khorixas (Fig. 1), a region that mapping and stratigraphic geometries [53, 59] indicate was a paleotopographic high (Makalani rim; Fig. 1) through the onset of Maieberg deposition. As such, this section is inferred to have been deposited in a shallower, and thus

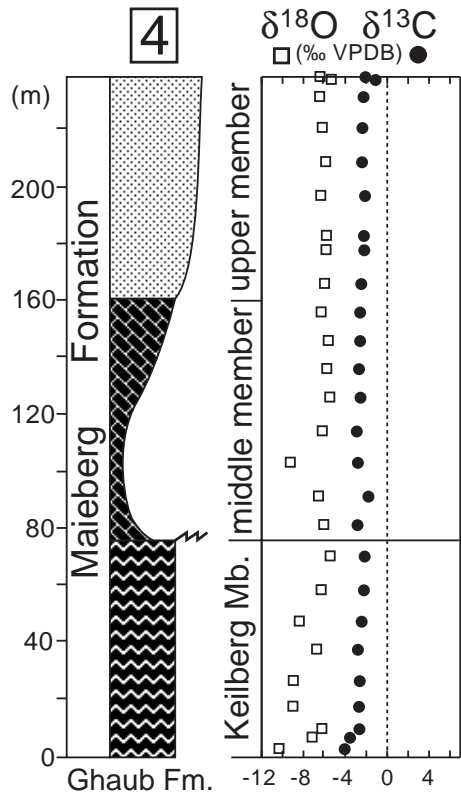


Fig. 5. Stratigraphic column and carbon and oxygen isotope data for Measured Section 4. Refer to Figure 3 for legend and see Supplementary Table 3 for tabulated data.

more restricted, environment than sections on the northern platform [19, 53]. The overall stratigraphy of the Maieberg Formation at MS-4 is similar to other Maieberg sections, with the exception that the Keilberg Member here is unusually thick (75 m) and the middle member is entirely dolomite. The  $\delta^{13}\text{C}$  and  $\delta^{18}\text{O}$  profiles through the Keilberg Member are also very similar to those in other sections, but this likeness disappears in the middle member, where neither  $\delta^{13}\text{C}$  nor  $\delta^{18}\text{O}$  change perceptibly. In fact, above the basal 10 m of the formation,  $\delta^{13}\text{C}$  remains virtually constant into the upper member, at  $\sim -2.5\text{‰}$ ;  $\delta^{18}\text{O}$  vary much less, and are on average more  $^{18}\text{O}$ -enriched than in northern platform sections.

Attempts to extract CAS from MS4 yielded no sulfate, indicating that the CAS concentrations in this section are extremely low. For this reason, we did not assess trace metal concentrations through this interval.

#### 4.4 Measured section 1

Measured section 1 (Fig. 6) is our northernmost section on the northern platform and is located near the village of Otjomatempa. Although the Maieberg

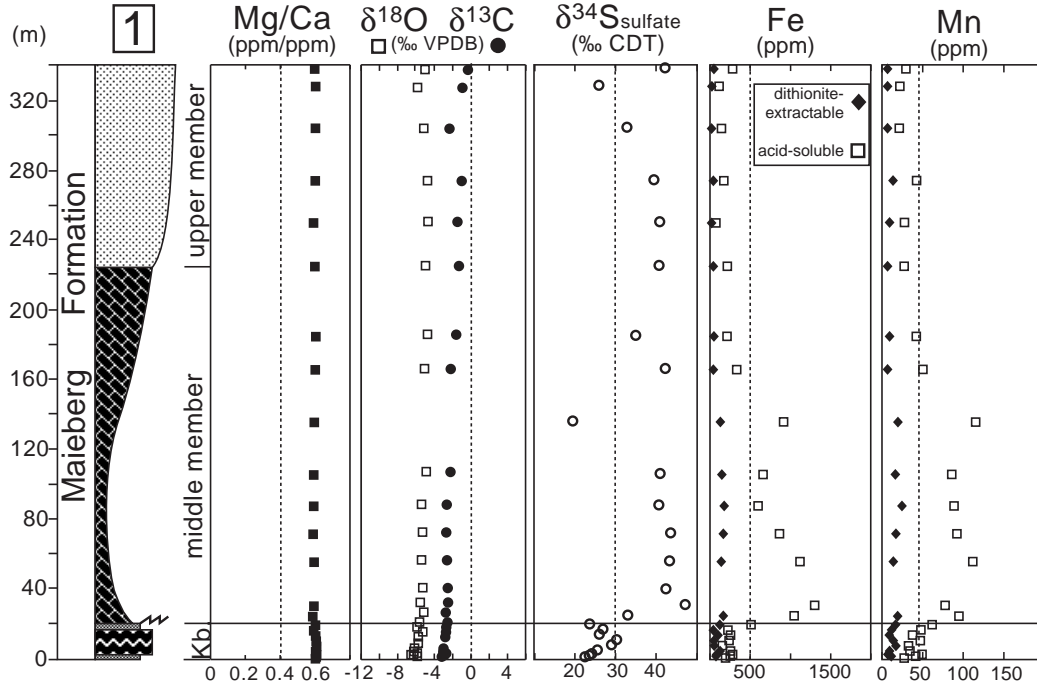


Fig. 6. Stratigraphic column and geochemical data from Measured Section 1. Refer to Figure 3 for legend, and see Supplementary Table 4 for tabulated data.

Formation here is somewhat thinner (325 m) than in sections to the south (Fig. 2), the underlying Abenab Subgroup is about 50% thicker than typical platform sections and the upper Ombaatjie Formation is unusually complete [53]. The Ghaub Formation is absent in this section, but continuous occurrences are found several kilometers to the south. Major facies changes also occur to the south, with debris flow beds and argillite in the upper Ombaatjie Formation and the appearance of the sheet-crack facies in the lower Maieberg Formation indicating a deepening depositional environment. At the same time, the Gruis and Ombaatjie Formations thin dramatically to the south.

Like MS-4, MS-1 is entirely dolomite, despite comprising the same sequence of facies as other typical platform sections. Similarly, the  $\delta^{13}\text{C}$  profile through the Maieberg Formation at MS-1 (Fig. 6) is virtually identical to that at MS-4 (Fig. 7), with the exception that  $\delta^{13}\text{C}$  rises to 0‰ by the top of the formation here, suggesting a more complete section. Both  $\delta^{13}\text{C}$  and  $\delta^{18}\text{O}$  are invariant across the top of the Keilberg Member. However,  $\delta^{34}\text{S}_{\text{sulfate}}$  values, which exhibit the familiar rise then fall in the Keilberg Member, increase abruptly by 25‰ at the base of the middle member (Fig. 6) and remain high ( $\sim 40\%$ ) into the upper member (with the exception of one point) sharply contrasting with the MS-3 and MS-8 sections where  $\delta^{34}\text{S}_{\text{sulfate}}$  declines abruptly at the base of the middle member (Fig. 7). Whereas overall  $\text{Fe}_{\text{carb}}$  and  $\text{Mn}_{\text{carb}}$  concentrations are substantially lower here than in MS-3 and MS-8, they show the same

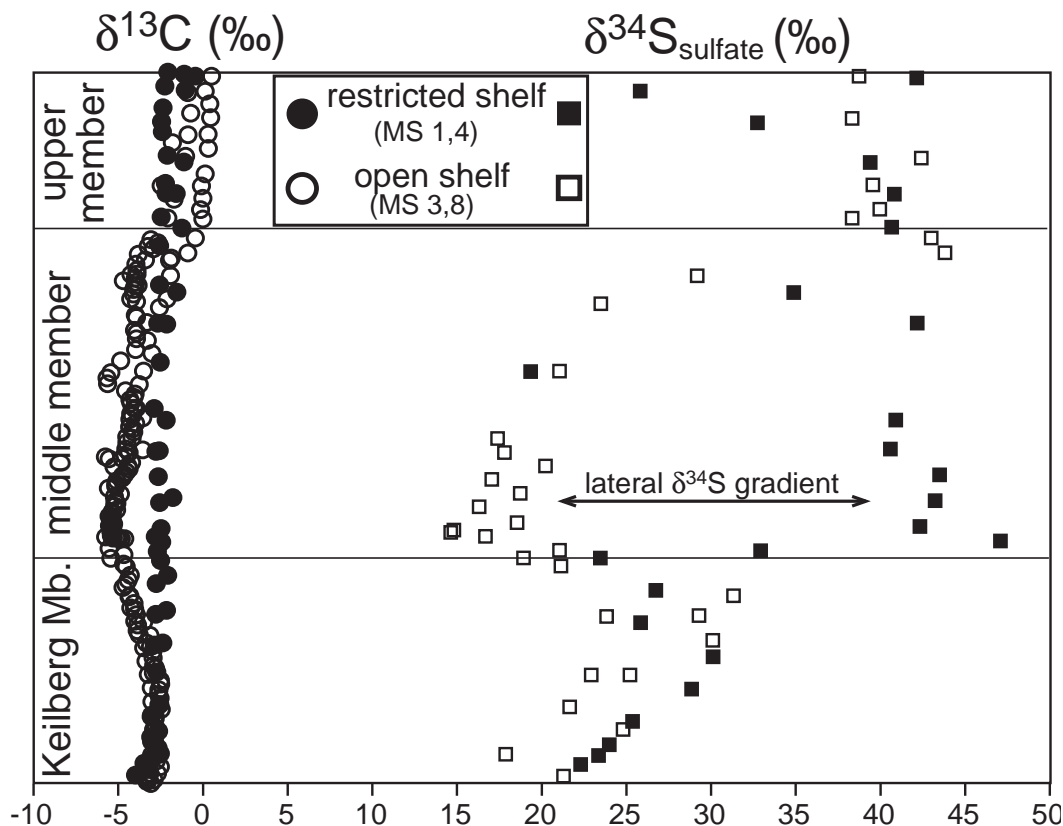


Fig. 7. Carbon and sulfur (sulfate) isotopic compositions for all four sections of the Maieberg Formation presented in this paper, separated into restricted- and open-shelf settings. The data are scaled to an arbitrary thickness for each of the three members to emphasize consistent and large variation in  $\delta^{34}\text{S}_{\text{sulfate}}$  in the Keilberg Member and a large difference  $\delta^{34}\text{S}_{\text{sulfate}}$  in the middle member between restricted and open shelf sections, which is interpreted to record a lateral chemical gradient on the Otavi platform. This gradient decays upsection, presumably recording homogenization of the ocean.  $\delta^{13}\text{C}$  compositions are also different between the inner shelf and shelf rim sections. While coupled shifts in  $\delta^{13}\text{C}$  and  $\delta^{13}\text{C}$  at the dolomite-limestone transition in MS-3,8 suggest that part of this signal is due to an equilibrium isotopic fractionation between calcite and dolomite.

pattern of a pulse to higher concentrations straddling the upper contact of the cap dolostone. Both  $\text{Fe}_{\text{ox}}$  and  $\text{Mn}_{\text{ox}}$  concentrations are relatively low and constant throughout this section.

## 5 Fidelity of sulfur isotope signatures

It is established that the  $\text{SO}_4^{2-}$  ion substitutes for the  $\text{CO}_3^{2-}$  ion in trace quantities in the carbonate crystal lattice [65], and carbonate-associated sulfate (CAS) is now routinely analyzed as a proxy for the  $\delta^{34}\text{S}$  of ancient seawater sulfate [e.g., 22, 23, 66, and references therein]. Burdett et al. [62] showed that CAS is incorporated into modern foraminifera from seawater with no isotopic

fractionation, and Kah et al. [32] demonstrated that  $\delta^{34}\text{S}_{sulfate}$  variations in dolomites of the 1.2 Ga Bylot Supergroup mirror those of coeval evaporite minerals. However, little systematic work has been carried out to monitor the effects of diagenesis and dolomitization or to test basin-scale reproducibility of  $\delta^{34}\text{S}_{sulfate}$  signatures. The large variations in  $\delta^{34}\text{S}_{sulfate}$  preserved in the Maieberg Formation warrant consideration of secondary processes that could affect the sulfur-isotope composition of ancient carbonates.

Burial diagenesis has been shown to decrease CAS concentrations [67]. Although sulfate loss alone should not change  $\delta^{34}\text{S}$  values, sulfur-isotope signatures will become progressively more susceptible to overprinting as CAS concentration decreases. Erez [68] has observed in laboratory experiments that CAS concentrations in foraminifera correlate positively with magnesium concentrations, presumably due to crystal lattice defects caused by incorporation of the  $\text{Mg}^{2+}$  ion. Although we cannot be certain that the same process operates during inorganic carbonate precipitation or dolomitization, we have observed qualitatively in Neoproterozoic rocks globally (unpublished data) that dolomite samples have, on average, greater CAS concentrations than limestone samples. Though seemingly at odds with the hypothesis that the sulfate ion inhibits dolomite formation [69], these observations present the possibility that carbonates might incorporate pore-water sulfate during dolomitization, which would be expected to be  $^{34}\text{S}$ -enriched compared to coeval seawater due to the effect of bacterial sulfate reduction (BSR) within a closed system. Such a process might account for the consistent  $^{34}\text{S}$ -enrichment ( $< \sim 4\text{‰}$ ) seen in the Bylot Supergroup dolomites compared to coeval evaporites [32].

The potential for  $^{34}\text{S}$ -enrichment during dolomitization raises the concern that the large difference ( $\sim 20\text{‰}$ ) in  $\delta^{34}\text{S}_{sulfate}$  between presumably coeval dolomite and limestone rhythmites above the Keilberg Member cap dolostone and the increase to very high  $\delta^{34}\text{S}_{sulfate}$  values in the upper Maieberg Formation (Fig. 7) reflect mineralogy and diagenetic processes rather than primary seawater signatures. However, even though we cannot eliminate the possibility that these highly  $^{34}\text{S}$ -enriched values have been modified by secondary processes, several lines of evidence suggest that the  $\delta^{34}\text{S}_{sulfate}$  data are essentially primary values. First, the structure of the  $\delta^{34}\text{S}_{sulfate}$  profile through the Keilberg Member is reproduced in all three sections for which we have data (Fig. 7), ruling out the possibility of wholesale overprinting of the Maieberg Formation. Second,  $\delta^{34}\text{S}_{sulfate}$  does not covary with CAS concentrations (Fig. 8a), as would be predicted if the secondary processes that altered CAS concentrations also introduced isotopically distinct sulfate into the carbonate. Similarly, variations in  $\delta^{34}\text{S}_{sulfate}$  do not correlate with  $\frac{\text{Mg}}{\text{Ca}}$  ratios (Fig. 8b), as would be expected if dolomitization exerted a strong control on the final  $\delta^{34}\text{S}$  signature preserved in the rocks. In fact, although the most  $^{34}\text{S}$ -enriched values do occur in the dolomite rhythmites and grainstones in the upper Maieberg Formation (Figs. 3, 4, 6), much of the rise in  $\delta^{34}\text{S}_{sulfate}$  ( $15\text{‰}$ ) in MS-8 occurs within the

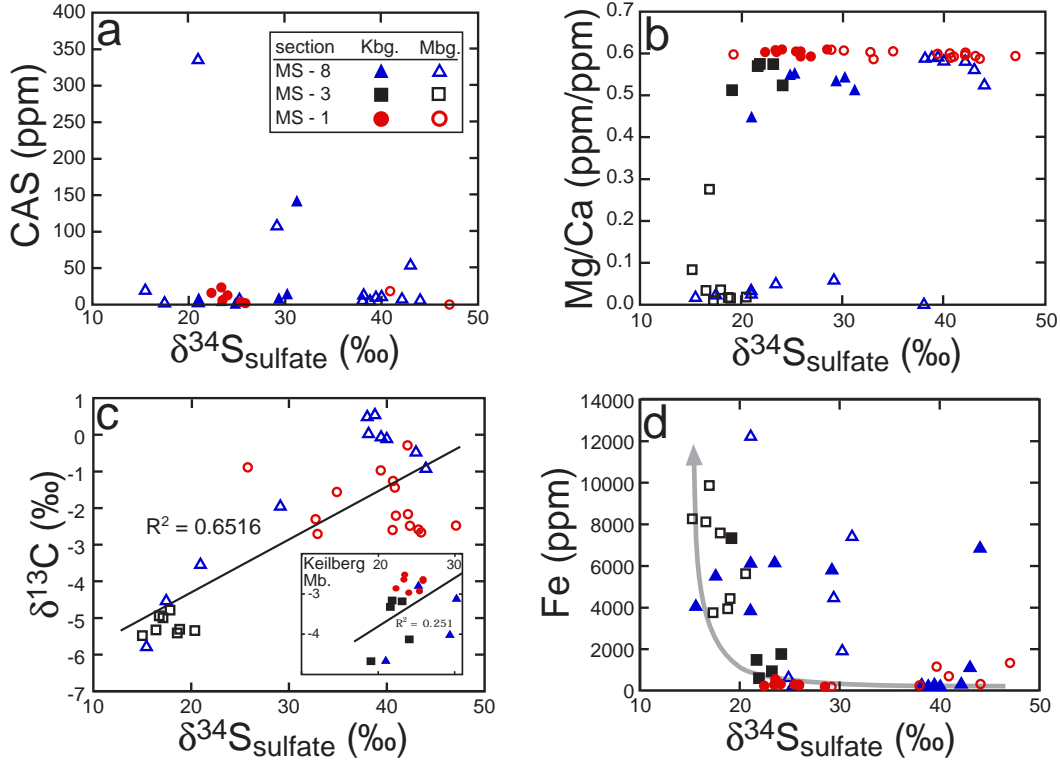


Fig. 8. Isotopic and elemental cross-plots for the Maieberg Formation for which sulfate data are available. In *a-c*, filled symbols represent data from the Keilberg Mb. (Kbg.) and open symbols data from the remainder of the Maieberg Fm. (Mbg.). **a,b** The absence of any correlation between  $\delta^{34}\text{S}_{\text{sulfate}}$  and either CAS or Mg/Ca suggests that the sulfur isotopic composition of CAS was not altered by post-depositional processes, including dolomitization, that decreased the concentration of trace sulfate within the carbonate lattice. **c**  $\delta^{34}\text{S}_{\text{sulfate}}$  and  $\delta^{13}\text{C}$  are moderately correlated in the Maieberg Formation, due to the coupled decreases in each proxy values spanning the upper Keilberg Member and middle member of MS3,8, but uncorrelated in the Keilberg Member as a whole (inset). **d** Cross-plot of  $\delta^{34}\text{S}_{\text{sulfate}}$  versus Fe concentration ( $\text{Fe}_{\text{carb}}$  only). Most data in the Maieberg Formation fall on or close to an approximate mixing curve (arrow) between low-Fe,  $^{34}\text{S}$ -enriched waters and high-Fe,  $^{34}\text{S}$ -depleted waters. The mixing curve suggests a  $\delta^{34}\text{S}$  composition of  $\sim 15\text{‰}$  in the latter, and an Fe concentration approaching nil in the former.

limestone member (Fig. 4). Although it would be ideal to confirm that the highly  $^{34}\text{S}$ -enriched pattern seen in the dolomitic middle member of MS-1 is reproducible in other all-dolomite sections, we note that the apparently extremely low (undetectable) CAS concentrations in MS-4, are consistent with the low concentrations in MS-1. A final argument against widespread alteration comes from an independent study (in a section on the northern platform, near our MS-2) that has demonstrated that the Maieberg Formation preserves presumably primary  $\delta^{11}\text{B}$  and  $\delta^{44}\text{Ca}$  signatures [70].

The decline in  $\delta^{34}\text{S}_{\text{sulfate}}$  at the base of the middle member in MS-3 (Fig. 3) and MS-8 (Fig. 4) corresponds to a decline in  $\delta^{13}\text{C}$ , accounting for the rough positive correlation between the two proxies (Fig. 8c), suggesting a link between the decline in  $\delta^{13}\text{C}$  and  $\delta^{34}\text{S}$  in the lower middle member. Likewise,

the onset of the decline in  $\delta^{34}\text{S}_{\text{sulfate}}$  in the Keilberg Member coincides with an increase in  $\text{Fe}_{\text{carb}}$  and  $\text{Mn}_{\text{carb}}$  concentrations, and the lowest  $\delta^{34}\text{S}_{\text{sulfate}}$  values occur in the lower part of the middle member, where  $\text{Fe}_{\text{carb}}$  and  $\text{Mn}_{\text{carb}}$  concentrations are on average highest (Figs. 3, 4). At face value, this pattern suggests that the fluids with elevated  $\text{Fe}^{2+}$  and  $\text{Mn}^{2+}$  concentrations were also relatively  $^{34}\text{S}$ -depleted, with  $\delta^{34}\text{S}$  approaching 15‰ (Fig. 8d). The increase in [Fe] and [Mn] also coincides with a coupled negative shift in  $\delta^{13}\text{C}$  and  $\delta^{18}\text{O}$  at the contact between the Keilberg Member and overlying limestone rhythmites (Figs. 3,4).

Whereas meteoric diagenesis could account for the elevated Mn and Fe concentrations and drop in  $\delta^{18}\text{O}$  at the contact between the dolomite and limestone, meteoric diagenesis seems unlikely in association with a transgressive event. Meteoric diagenesis could have occurred much later, for example as a result of orogenically-driven groundwater flow utilizing the middle member as an aquifer. However, the reproducibility of negative shifts in both  $\delta^{13}\text{C}$  and  $\delta^{18}\text{O}$  throughout the Otavi platform and in Marinoan cap carbonates in general [19] argues against a diagenetic origin for these geochemical signals at the dolomite-limestone transition. In fact, the paired isotopic shifts in  $\delta^{13}\text{C}$  and  $\delta^{18}\text{O}$  at the dolomite-limestone transition are consistent with an equilibrium isotope fractionation between the two carbonate phases [40], with both carbon and oxygen being isotopically heavier in the dolomite. Since secondary dolomite could inherit its  $\delta^{13}\text{C}$  composition from the calcite (or aragonite) precursor [71], and assuming that the limestone was precipitated from seawater, the carbon-isotopic difference between dolomite and limestone could be preserved if the dolomite was primary or if it formed penecontemporaneously with deposition, while still in equilibrium with seawater. While equilibrium isotope fractionation between dolomite and calcite can partly explain the negative shift in  $\delta^{13}\text{C}$  and  $\delta^{18}\text{O}$  at the dolomite-limestone transition, additional mechanisms will be discussed below. Nevertheless, the mechanism responsible for the shift from dolomite to calcite or aragonite precipitation is temporally and most likely causally linked to that responsible for the spike in [Fe] and [Mn] at the same level. The invariant  $\delta^{13}\text{C}$  spanning the upper contact of the Keilberg Member in MS-1 and MS-5, coupled with subtle changes in [Mn] and [Fe] (Fig. 7), implies that the all-dolomite Maieberg sections are not simply dolomitized equivalents of typical limestone sections. Rather, primary or early dolomite precipitation may have continued in shallower and more restricted settings after deposition of the Keilberg Member.

Lacking a straightforward diagenetic mechanism to explain the unusual isotope geochemistry of the Maieberg Formation, we explore the implications for the evolution of seawater chemistry in the aftermath of the Marinoan glaciation based on the assumption that these are near-primary marine signatures.

## 6 Interpretation of geochemical signals

$\delta^{34}\text{S}_{\text{sulfate}}$  at the base of the Keilberg cap dolostone is  $\sim 20\%$ . This unspectacular value is nearly the same as that preserved in the equivalent Nuccaleena cap dolostone in South Australia [31] and as present seawater. Given that  $[\text{SO}_4^{2-}]$  may have been greatly diminished during a snowball Earth event [22], the sulfur isotope composition of CAS preserved in the cap dolostone likely represents contributions of sulfur from several sources including volcanically derived  $\text{SO}_2$ , sulfur species trapped within ice and released during glacial meltback and the weathering of sulfides and release of trace sulfate during the dissolution of platform carbonates (i.e., the Abenab Subgroup), which were exposed as a result of glacial sea level fall [50]. The dissolution of exposed carbonates may have also contributed a significant portion of the alkalinity for cap dolostone precipitation [40].

What is interesting about the  $\delta^{34}\text{S}_{\text{sulfate}}$  record of the Keilberg Member is the increase of  $\sim 10\%$  that occurs in the lower four-fifths of the unit, followed by a decline of equal magnitude at the very top of the dolostone (Fig. 7). Although the absolute  $\delta^{34}\text{S}_{\text{sulfate}}$  values are not identical in all sections, the trend is virtually the same (Fig. 7), which suggests that the cap dolostone was precipitated from a water mass of roughly uniform chemical composition with respect to sulfate, at least at the basinal scale. Since the Keilberg Member was deposited entirely within the period of post-glacial transgression, which is hypothesized to have been very rapid [ $\sim 2000$  years; 72], the rise in  $\delta^{34}\text{S}_{\text{sulfate}}$  must reflect low initial  $[\text{SO}_4^{2-}]$  and either the input of  $^{34}\text{S}$ -enriched sulfate to the surface ocean, or the removal of  $^{34}\text{S}$ -depleted sulfur from the surface ocean (or some combination of both). One source of  $^{34}\text{S}$ -enriched sulfate may have been the oxidation of sulfide minerals from the underlying Ombaatjie Formation, which was exposed as a result of glacial sea level fall. While sulfide sulfur isotope data are not available from the Ombaatjie Formation, Gorjan et al. [25] identified isotopically enriched pyrite from the pre-glacial Trezona Formation in South Australia, with values reaching  $18\%$ . One could also interpret the pattern of increasing  $\delta^{34}\text{S}$  in terms of the removal of isotopically light sulfur—most likely as a result of BSR and subsequent sulfide burial. The *initial* rise in  $\delta^{34}\text{S}_{\text{sulfate}}$  within the Keilberg Member does not correlate with changes in any other geochemical proxies, most notably  $\delta^{13}\text{C}$  (Fig. 8c), and therefore is probably not related to the oxidation of methane, which has been suggested by some authors [61, 73] to be a quantitatively important process controlling the carbon-isotopic composition of the cap dolostones.

The most intriguing result from this study is the decline in  $\delta^{34}\text{S}_{\text{sulfate}}$  at the top of the Keilberg Member and the geochemical disparities that develop laterally on the Otavi platform beginning at the transition between the Keilberg and middle members. Unlike the preceding increase in  $\delta^{34}\text{S}_{\text{sulfate}}$ , the sulfur

isotope decrease at the top of the Keilberg Member corresponds to marked increases in  $\text{Fe}_{carb}$  and  $\text{Mn}_{carb}$  and to a lesser extent  $\text{Fe}_{ox}$  and  $\text{Mn}_{ox}$  (Figs. 3, 4). The decrease in  $\delta^{34}\text{S}_{sulfate}$  continues into the overlying middle member in open shelf sections (MS-3 and MS-8), where the lower rhythmite is limestone and  $\delta^{34}\text{S}_{sulfate}$  drops as low as 15‰. However, in MS-1, where the lower middle member is dolomite,  $\delta^{34}\text{S}_{sulfate}$  shows the opposite trend, jumping to >40‰ (Fig. 7). This large lateral  $\delta^{34}\text{S}$  gradient develops in step with iron and manganese enrichment and at the same stratigraphic level in which seafloor barite occurs in other settings. These combined observations imply that a water mass rich in Ba and reduced metal species (Fe and Mn), and therefore anoxic, impinged onto the Otavi platform during the transgression. The anoxic deep water would have been overlain by the surface mixed layer that was dominated by the buoyantly stable glacial meltwater that furnished the rise in sea level, and was well oxygenated, assuming the atmosphere contained  $\text{O}_2$ . The boundary between these two water masses would have been a redox chemocline, not unlike that which exists beneath the surface layer of the modern Black Sea.

$\delta^{34}\text{S}_{sulfate}$  first drops in the upper cap dolostone where [Fe] and [Mn] begin to increase, implying that the transgression also introduced relatively  $^{34}\text{S}$ -depleted sulfur to the outer Otavi platform. But if the trace metals were derived from an anoxic deep ocean, what was the source of  $^{34}\text{S}$ -depleted sulfur to the open shelf sections? A critical clue is the seafloor barite, which formed regionally extensive crusts atop cap dolostones in northwest Canada [12] and central Australia. Because barite is extremely insoluble within seawater, barium and sulfate ions cannot coexist within the same water mass. Therefore, it is unlikely that  $^{34}\text{S}$ -depleted sulfur existed as sulfate within the deep ocean, otherwise barium would have been titrated from the deep sea as barite, as it is today. A tempting explanation is that the deep ocean was euxinic (anoxic + sulfidic) and the sulfate preserved in the middle member limestone was derived from oxidation in the chemocline of sulfide residual from the snowball glaciation (Fig. 9b). Bearing in mind that no fractionation accompanies the direct oxidation of sulfide to sulfate, this hypothesis is supported by the nearly identical  $\delta^{34}\text{S}$  composition of coeval CAS and pyrite in MS-8 (Fig. 4). Whereas the lack of difference in  $\delta^{34}\text{S}$  between sulfate and pyrite could be taken to reflect BSR under extremely low sulfate concentrations [ $< 0.2$  mM; 74], the preservation of CAS in the middle member limestone suggests that  $[\text{SO}_4^{2-}]$ , while low, were not low enough to merit this interpretation.

Most, if not all, of the marine sulfate reservoir would have been consumed via BSR during the snowball glaciation [22]. Consequently, assuming quantitative conversion of sulfate to sulfide, the average sulfur isotope composition of the sulfide derived from BSR of the marine sulfate reservoir would have been equal to the initial (pre-glacial) sulfur isotope composition of marine sulfate. While it is not clear what the pre-glacial sulfur isotope composition of seawater

ter sulfate was,  $\delta^{34}\text{S}_{\text{sulfate}}$  falls between 13 and 28‰ in the upper Ombaatjie Formation [22] and 26 to 29‰ in the Trezona Formation of South Australia [31], with a discernible upward positive trend. These values are on average much higher than the <20‰ values preserved as CAS in limestone sections of the middle member. Therefore, it seems another, isotopically depleted source of sulfide must have contributed to the snowball sulfide reservoir. The most obvious source of  $^{34}\text{S}$ -depleted sulfur is mantle-derived sulfur ( $\sim 0\%$ ) entering the snowball ocean from hydrothermal vents. In the modern ocean, the hydrothermal sulfur flux to the ocean is minor compared to the riverine flux [26], but during a snowball glaciation, the riverine sulfate flux may have been greatly reduced [22], and over the course of 5 to 30 Myr. [e.g., 6, 75], the hydrothermal sulfide flux would have been quantitatively important.

During the deglacial transgression, the chemocline between the deep anoxic waters and surface mixed layer would have been dynamic, its intersection with the seafloor migrating up the Otavi platform (Fig. 9c). However, since the rise in sea level was driven by the addition of glacial melt water to the ocean, the transgression was accomplished by adding water to the surface mixed layer, not by raising the level of the original deep water. Furthermore, during the transgression, the mixed layer was unusually thick (200 - 400 m), perhaps twice as thick as the mixed layer in the modern ocean due to ongoing, severe storms in the aftermath of the glaciation [10]. These factors combined would have prevented the cold anoxic water mass from advancing far up the continental shelf, with the consequence that over the course of the transgression, the thermohaline and redox gradients would have been attenuated along some continental margins, except in regions of strong upwelling. The restriction of the cold, anoxic water mass to the outer shelf and beyond would have set up the large lateral chemical gradients across the continental platform observed in the  $\delta^{34}\text{S}_{\text{sulfate}}$  (Fig. 7), CAS concentration, and [Fe] and [Mn] data. This would also explain why barite cements are not more widespread, since they would be expected to form only where the anoxic waters were in contact with the surface ocean, a condition that would have only been met on the outer shelf or upper foreslope, early during the transgressive phase, before the contact between the mixed layer and the seafloor had migrated far up the continental shelf.

These lateral variations are broadly mirrored by the mineralogy of the middle member of the Maieberg Formation, with more distal, open ocean sections being limestone at the base and restricted and shallow sections dolomite (Fig. 2). Insofar as the sulfate ion exerts a primary control on dolomite precipitation, either directly by inhibiting dolomite nucleation [69], or indirectly through mediation by sulfate-reducing bacteria [76], this pattern is consistent with lateral gradients in sulfate concentration. That is, in open ocean sections, closer to the predominant source of sulfate, the sulfate concentration (CAS up to 335 ppm) was sufficient to prevent dolomite precipitation, while

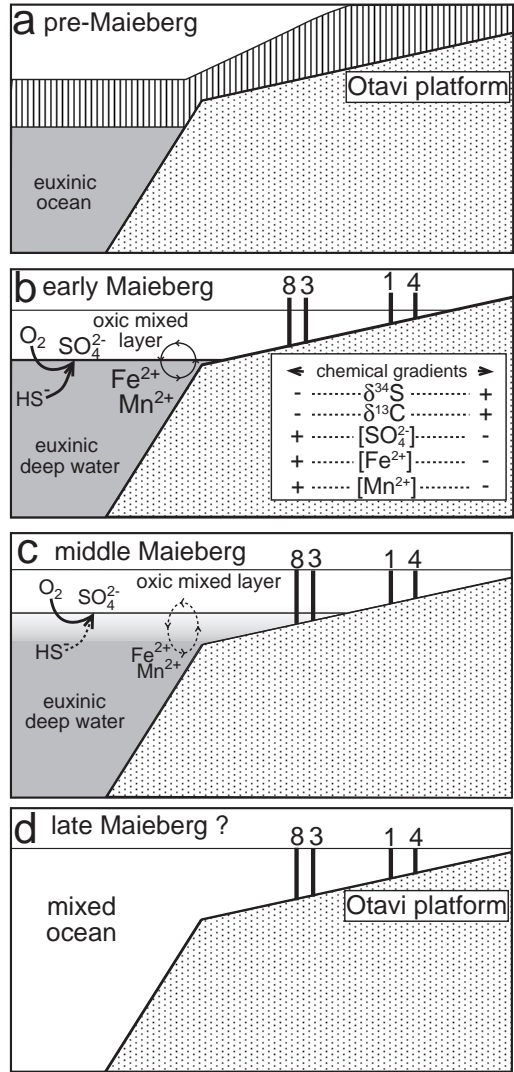


Fig. 9. A conceptual model for the chemical evolution of seawater along the Otavi Platform during deposition of the Maieberg Formation cap carbonate. **a** At the end of the snowball glaciation, the ocean is sealed in sea ice and the Otavi Platform is depressed beneath a continental ice shelf. **b** During the early deglaciation stage (lower Keilberg Member), the ocean is divided into a deep, cold, anoxic (euxinic) water mass relict from the snowball glaciation and a surface, oxidized mixed layer dominated by melt water from sea and glacier ice. Intense redox cycling along the strong chemocline between the two water masses is restricted to the open ocean; Fe and Mn are concentrated in the chemocline and sulfate is produced by oxidation of deep water sulfide. **c** As sea level rises due to continued melting of continental glaciers, the mixed layer transgresses the platform. However, since the cold deep waters do not rise and the mixed layer is rendered unusually deep due to extremely stormy weather [10], the deep waters do not similarly transgress the platform. As a result, surface-to-deep gradients attenuate, and strong lateral chemical gradients develop across the platform, with sulfate, Fe, and Mn concentrations increasing towards the continental margin, where the chemocline is strongest and the sea bed lies below the mixed layer. **a** Stratification on the Otavi platform eventually decays, perhaps by late Maieberg times, during which time the geochemical gradients along the platform disappear. However, shoaling of the platform, due to a combination of isostatic uplift and rapid deposition rates, may also have contributed to this signal, by elevating the level of the sea bed above the base of the mixed layer.

in more restricted and shallower settings, where sulfate concentrations were exceedingly low (CAS < 25 ppm), primary or early dolomite precipitation continued above the cap dolostone. The sharp spike in  $\delta^{34}\text{S}_{\text{sulfate}}$  above the cap dolostone therefore likely records Rayleigh distillation of the small sulfate reservoir in the restricted surface ocean, due to isotopic fractionation during ongoing BSR. The Maieberg dolomites are exceedingly sparse in organic matter, but little would have been necessary to draw down the inferred low concentration of available sulfate.

It is noteworthy that the decline in  $\delta^{34}\text{S}_{\text{sulfate}}$  at the top of the cap dolostone, broadly correlates with a decline in  $\delta^{13}\text{C}$  in open ocean sections (Fig. 8c). We have argued that part of this change can be attributed to the equilibrium isotope fractionation between calcite and dolomite [cf. 40], based on the coupled decline in  $\delta^{18}\text{O}$  across the dolomite-limestone transition (Figs. 3,4). However, the combination of the gradual decrease in  $\delta^{13}\text{C}$  beginning in the middle of the cap dolostone and the  $\sim 3\text{‰}$  difference in  $\delta^{13}\text{C}$  that develops between the limestone and dolomite sections in the lower middle member (Fig. 7), which is greater than the 1 – 2‰ difference from fractionation alone [77], suggest that this signal is at least partly influenced by mixing with a  $^{13}\text{C}$ -depleted reservoir of dissolved inorganic carbon (DIC). If the decline in  $\delta^{34}\text{S}_{\text{sulfate}}$  is the result of oxidation of deep-water sulfide, then it follows that the isotopically light carbon is also derived from the deep ocean. This idea is supported by documentation of gradients of up to 3‰ between inner shelf and basinal facies of the Doushantuo Formation [42], which are interpreted to record depth gradients in a stratified ocean following the Marinoan glaciation [43].

Deep water  $^{13}\text{C}$ -depletion may have resulted from the oxidation of organic carbon to bicarbonate via BSR. Assuming that organic carbon was the only substrate used during BSR (e.g., no BSR via  $\text{H}_2$ ) and that 1 mM of sulfate ( $1.37 \times 10^{18}$  moles of S) was consumed during the glacial event, then  $2.74 \times 10^{18}$  moles of  $^{13}\text{C}$ -depleted bicarbonate would have been produced. If the  $\delta^{13}\text{C}$  of the organic carbon used to fuel BSR was -25‰ during the glacial event and assuming the ocean contained 5 to 10 times more DIC than today [40], then deep water  $\delta^{13}\text{C}$  values may have shifted by -2 to -3‰. While this simple calculation is based on estimates of mostly unknown quantities for this time period ( $[\text{SO}_4^{2-}]$ ,  $[\text{DIC}]$ , substrate fueling BSR,  $\epsilon_p$ ), it illustrates that the observed geochemical gradients are not unreasonable given the model developed above. A gradient between the surface and deep oceans during the post-glacial transgression is hardly surprising, even if the ocean was isotopically homogeneous during the glaciation, since surface ocean  $\delta^{13}\text{C}$  would have been effected by equilibration with a  $\text{CO}_2$ -charged atmosphere [6] and input of DIC from carbonate and silicate weathering [40]. The  $\delta^{18}\text{O}$  gradient between open ocean and more restricted settings is more difficult to interpret. The surface mixed layer generated during deglaciation and dominated by meltwater from sea and glacier ice, should have been  $^{18}\text{O}$ -depleted. However, the opposite trend

is observed; open ocean settings are characterized by lighter  $\delta^{18}\text{O}$ .

Nevertheless, the lateral geochemical gradient along the Otavi platform would have been maintained as long as the waters along this particular continental margin remained stratified. Given the presumed sharp density contrast between the cold, saline, deep ocean and the much warmer and brackish surface ocean, stratification on the Otavi platform could have persisted beyond the end of the transgression. The disappearance of the  $\delta^{34}\text{S}$  difference between the restricted and open shelf settings in the upper Maieberg Formation (Fig. 7) and the decay of the elevated Fe and Mn concentrations in MS3,8 suggest that platform waters may have finally mixed by the beginning of deposition of the upper member of the Maieberg Formation (Fig. 9d). However, this signal may equally have resulted from the offshore migration of the chemocline as relative sea level dropped due to a combination of aggradation of the carbonate platform (recorded in the shoaling-upward facies) and glacio-isostatic uplift [50]. Therefore, given the present data, it is difficult to determine precisely when stratification ended. Sulfur isotope analysis of Tsumeb Subgroup-equivalent carbonates from upper foreslope sections (Karibib Formation) could provide an answer to this question.

One problem with the proposed model for the geochemistry of the Maieberg Formation (Fig. 9) is the concurrence of the signal of sulfur input from the deep ocean with a peak in iron concentrations, since  $\text{Fe}^{2+}$  and sulfide cannot coexist in appreciable amounts within the same water mass as they react to form Fe sulfide minerals. However, Fe concentrations are still significantly higher (10-100 times) in modern euxinic environments (such as the Black Sea) than the open ocean [78]. Furthermore, in the Black Sea and other water bodies with strong redox gradients, reduced Fe concentrations are greatest at or near the chemocline [e.g., 79]. Fe is cycled within the chemocline, both biotically and abiotically, between oxidized and reduced forms and spatially isolated from deeper parts of the water column where sulfide concentrations are greatest [80]. Therefore, the high Fe concentrations in the acid-soluble component of carbonates in transition at the top of the cap dolostone may record elevated levels in the chemocline rather than high concentrations of  $\text{Fe}^{2+}$  in the deep ocean. This explanation is consistent with the Fe and Mn spike at the top of the cap dolostone being a diachronous rather than instantaneous signal, recording the migration of the chemocline up the continental shelf.

Additional sources of iron and manganese in the chemocline may include recycled sulfide minerals from shelf and foreslope sediments. Oxidation of sulfide minerals in contact with the chemocline [e.g., 81, 82] could have provided a source of Fe and Mn, which could have been particularly important early in the transgression, prior to the burial of the glacial and pre-glacial sediments beneath the cap carbonate. Oxidation of iron and manganese, in turn, could have also contributed to the spike in  $\text{Fe}_{ox}$  and  $\text{Mn}_{ox}$  at the top of the cap dolo-

stone. Another potentially important source of  $\text{Fe}_{ox}$  would have been the flocculation and subsequent sinking of river-borne clays and Fe(III)-oxyhydroxide colloids as the surface mixed layer mixed with the saline deep waters. Just as flocculation in estuaries removes most river-borne Fe from the oceans, the coagulation of Fe-rich particles in the mixing zone between the deep and surface layers would have been a major sink for Fe derived from glacial runoff, contributing to, if not dominating, the spike in  $\text{Fe}_{ox}$  concentrations.

## 7 Conclusions

The geochemical signatures preserved within the Maieberg Formation, as determined from coeval sections representing both open-ocean and more restricted settings, suggest that Otavi platform waters were stratified in the immediate aftermath of glaciation, in which cold, euxinic deep water was overlain by a warm, oxic, and brackish surface layer.  $\delta^{34}\text{S}_{sulfate}$  values from both basin margin and more restricted settings are broadly similar through the Keilberg Member, suggesting that the cap dolostone precipitated from a water mass of roughly comparable chemical composition. These values show large and rapid changes indicating extremely low sulfate concentrations in the surface mixed layer, from which the cap dolostone precipitated. The transition between the Keilberg Member and overlying middle member is marked by a spike in Fe and Mn concentrations in both carbonate and oxy-hydroxide phases, as well as the development of a large disparity in  $\delta^{34}\text{S}_{sulfate}$  across the Otavi platform, which persists through middle member, and a decline in  $\delta^{13}\text{C}$  in open shelf sections. We interpret the  $\delta^{34}\text{S}_{sulfate}$  low values ( $<20\%$ ) in open ocean sections, closer to the shelf margin, to record the input of sulfate derived from the oxidation of deep-ocean sulfide, and the high ( $>40\%$ ) values in more restricted sections to reflect ongoing BSR in a waters with very low sulfate concentrations. The pulse in Fe and Mn concentrations, which decreases in magnitude shoreward, likely records the up-slope migration and attenuation of the chemocline during the transgression. The decline in  $\delta^{13}\text{C}$  at the top of the Keilberg Member in MS-3 and MS-8 and the  $\sim 3\%$  difference between limestone in open shelf sections and dolomite in restricted sections (Fig. 7) is interpreted to record the combination of an equilibrium isotope effect between coeval dolomite and calcite and the input of  $^{13}\text{C}$ -depleted deep-water DIC to the surface ocean at the shelf margin.

The sulfur isotope data from the Maieberg Formation have important implications for the reconstruction of the Neoproterozoic  $\delta^{34}\text{S}$  record and the timing of the growth of the marine sulfate reservoir. If, as the data imply, large lateral  $\delta^{34}\text{S}$  gradients developed in the aftermath of the Marinoan glaciation, then it is clear that sulfur isotopic evolution of sea water following glaciations, and perhaps other major climatic perturbations, cannot be reconstructed from a

single stratigraphic section. Instead, multiple sections from a transect perpendicular to the paleo-shoreline are necessary to test for the non-steady state evolution of the sulfur isotopic composition of the sulfate reservoir and to establish the range of seawater  $\delta^{34}\text{S}_{\text{sulfate}}$  [see also 83, 84]. The data presented herein also suggest that  $\delta^{34}\text{S}$  data from post-glacial carbonates cannot be easily used as a tool for making global correlations. Additional work is necessary to test the variability of CAS  $\delta^{34}\text{S}$  data in carbonates not associated with deglaciation to determine whether or not these are more suitable for the purpose of correlations and to test whether a sulfidic deep ocean was the norm for the Neoproterozoic.

The evidence for the complete removal of sulfate from the ocean during the Marinoan glaciation indicates that the marine sulfate reservoir did not simply increase gradually from the late Mesoproterozoic to the early Paleozoic. Less sulfur isotope data is available from carbonates deposited following the Sturtian and Gaskiers glaciations, but the possibility that sulfate concentrations also plummeted during these events must be considered. Much more data from multiple successions and spanning the entire Neoproterozoic and into the Paleozoic is necessary to be able to 1) establish the sulfur isotopic composition and size of the sulfate reservoir prior to glaciation, and thus deduce the environmental impact of the glaciations, 2) compare the sulfur isotopic evolution of the oceans following the three glaciations, and, 3) determine when the sulfate reservoir finally grew to near modern levels. However, the presently available data are sufficient to demonstrate the late Proterozoic growth of the marine sulfate reservoir, and by implication, the oxidation of the Earth's surface environment, was accomplished in fits and bursts.

## 8 Acknowledgments

This project was funded by the NASA Astrobiology Institute (NCC2-1057), National Science Foundation (Earth System History), Harvard University, CIAR (Earth System Evolution Project), and the Geological Survey of Namibia. We thank Y. Shen and an anonymous review for comments that improved the content and clarity of this manuscript.

## References

- [1] B. Embleton, G. Williams, Low palaeolatitude of deposition for late Precambrian periglacial varvites in South Australia: implications for paleoclimatology, *Earth and Planetary Sciences Letters* 79 (1986) 419–430.
- [2] P. Schmidt, G. Williams, The Neoproterozoic climatic paradox: equatorial paleolatitudes for Marinoan glaciation near sea level in South Australia, *Earth and Planetary Sciences Letters* 134 (1995) 107–124.
- [3] L. Sohl, N. Christie-Blick, D. Kent, Paleomagnetic polarity reversals in Marinoan (ca. 600 ma) glacial deposits of Australia: Implications for the duration of low-latitude glaciations in Neoproterozoic time, *Geological Society of America Bulletin* 111 (1998) 1120–1139.
- [4] D. Evans, Stratigraphic, geochronological, and paleomagnetic constraints upon the Neoproterozoic climatic paradox, *American Journal of Science* 300 (2000) 262–266.
- [5] J. Kirschvink, Late Proterozoic low-latitude glaciation: The snowball Earth, in: J. Schopf, C. Klein (Eds.), *The Proterozoic Biosphere*, Cambridge University Press, 1992, pp. 51–52.
- [6] P. Hoffman, A. Kaufman, G. Halverson, D. Schrag, A Neoproterozoic snowball Earth, *Science* 281 (1998) 1342–1346.
- [7] Y. Donnadieu, Y. Godd eris, G. Ramstein, A. N edelec, J. Meert, A ‘snowball earth’ climate triggered by continental break-up through changes in runoff, *Nature* 428 (2004) 303–306.
- [8] D. Pollard, J. Kasting, Climate-ice sheet simulations of Neoproterozoic glaciation before and after collapse to Snowball Earth, in: G. Jenkins, M. McMenamin, C. McKey, L. Sohl (Eds.), *The Extreme Proterozoic: Geology, Geochemistry, and Climate*, Vol. Geophysical Monograph 146, American Geophysical Union, Washington, DC, 2004, pp. 91–105.
- [9] W. Peltier, L. Tarasov, G. Vettoretti, L. Solheim, Climate dynamics in deep time: modeling the “snowball bifurcation” and assessing the plausibility of its occurrence, in: G. Jenkins, M. McMenamin, C. McKey, L. Sohl (Eds.), *The Extreme Proterozoic: Geology, Geochemistry, and Climate*, Vol. Geophysical Monograph 146, American Geophysical Union, Washington, DC, 2004, pp. 107–124.
- [10] P. A. Allen, P. F. Hoffman, Extreme winds and waves in the aftermath of a Neoproterozoic glaciation, *Nature* 433 (2005) 123–127.  
URL <http://dx.doi.org/10.1038/nature03176>
- [11] R. Pierrehumbert, High levels of atmospheric carbon dioxide necessary for the termination of global glaciation, *Nature* 429 (2004) 646–649.
- [12] P. Hoffman, D. Schrag, The snowball Earth hypothesis: testing the limits of global change, *Terra Nova* 14 (2002) 129–155.
- [13] G. Williams, Sedimentology, stable-isotope geochemistry and palaeoenvironment of dolostones capping late Precambrian glacial sequences in Australia, *Journal of the Geological Society of Australia* 26 (1979) 377–386.

- [14] I. Fairchild, Balmy shores and icy wastes: the paradox of carbonates associated with glacial deposits in Neoproterozoic times, *Sedimentology Review* 1 (1993) 1–16.
- [15] J. Grotzinger, A. Knoll, Anomalous carbonate precipitates: Is the Precambrian the key to the Permian?, *Palaios* 100 (1995) 578–596.
- [16] M. Kennedy, Stratigraphy, sedimentology, and isotopic geochemistry of Australian Neoproterozoic postglacial cap dolostones: Deglaciation,  $\delta^{13}\text{C}$  excursions, and carbonate precipitation, *J. Sed. Res.* 66 (6) (1996) 1050–1064.
- [17] N. James, G. Narbonne, T. Kyser, Late Neoproterozoic cap carbonates: Mackenzie Mountains, northwestern Canada: precipitation and global glaciation, *Canadian Journal of Earth Science* 38 (2001) 1229–1262.
- [18] P. Hoffman, A. Kaufman, G. Halverson, Comings and goings of global glaciations on a Neoproterozoic tropical platform in Namibia, *GSA Today* 8 (1998) 1–9.
- [19] G. Halverson, P. Hoffman, D. Schrag, A. Maloof, A. Rice, Towards a Neoproterozoic composite carbon isotope record, *Geological Society of America Bulletin* 117 (2005) 1181–1207.
- [20] D. Condon, M. Zhu, S. Bowring, W. Wang, A. Yang, Y. Jin, U-Pb ages from the Neoproterozoic Doushantuo Formation, China, *Science* 308 (2005) 95–98.
- [21] K.-H. Hoffmann, D. Condon, S. Bowring, J. Crowley, A U-Pb zircon date from the Neoproterozoic Ghaub Formation, Namibia: Constraints on Marinoan glaciation, *Geology* 32 (2004) 817–820.
- [22] M. Hurtgen, M. Arthur, N. Suits, A. Kaufman, The sulfur isotopic composition of Neoproterozoic seawater sulfate: implications for snowball Earth?, *Earth and Planetary Science Letters* 203 (2002) 413–429.
- [23] M. Hurtgen, M. Arthur, A. Prave, The sulfur isotopic composition of carbonate-associated sulfate in Meso- to Neoproterozoic carbonates from Death Valley, CA, in: J. Amend, K. Edwards, T. Lyons (Eds.), *Sulfur Biogeochemistry-Past and Present*, Vol. 379 of Geological Society of America Special Paper, Geological Society of America, 2004, pp. 177–94.
- [24] G. Ross, J. Bloch, H. Krause, Neoproterozoic strata of the southern Canadian Cordillera and the isotopic evolution of seawater sulfate, *Precambrian Research* 73 (1995) 71–79.
- [25] P. Gorjan, J. Veevers, M. Walter, Neoproterozoic sulfur-isotope variation in Australia and global implications, *Precambrian Research* 100 (2000) 151–179.
- [26] W. Holser, J. Maynard, K. Cruikshank, in: P. Brimblecombe, A. Yu (Eds.), *Evolution of the Global Biogeochemical Sulfur Cycle*, Wiley, New York, NY, 1989, pp. 21–56.
- [27] C. Rees, W. Jenkins, J. Monster, The sulphur isotopic composition of ocean water sulphate, *Geochimica et Cosmochimica Acta* 428 (1978) 377–381.
- [28] D. Canfield, Isotope fractionation by natural populations of sulfate-

- reducing bacteria, *Geochimica et Cosmochimica Acta* 65 (2001) 1117–1124.
- [29] M. Raab, B. Spiro, Sulfur isotopic variations during seawater evaporation with fractional crystallization, *Chemical Geology* 86 (1991) 323–333.
- [30] A. Paytan, M. Kastner, D. Campbell, M. Thiemens, Sulfur isotopic composition of Cenozoic seawater sulfate, *Science* 282 (1998) 1459–1462.
- [31] M. Hurtgen, M. Arthur, G. Halverson, Neoproterozoic sulfur isotopes, the evolution of microbial sulfur species, and the burial efficiency of sulfide as sedimentary pyrite, *Geology* 33 (2005) 41–44.
- [32] L. Kah, T. Lyons, T. Frank, Low marine sulphate and protracted oxygenation of the Proterozoic biosphere, *Nature* 431 (2004) 834–838.
- [33] C. Fanning, P. Link, U-Pb shrimp ages of Neoproterozoic (Sturtian) glaciogenic Pocatello Formation, southeastern Idaho, *Geology* 32 (2004) 881–884.
- [34] M. Brasier, G. McCarron, R. Tucker, J. Leather, P. Allen, G. Shields, New U-Pb zircon dates for the Neoproterozoic Ghubrah glaciation and for the top of the Huqf Supergroup, Oman, *Geology* 28 (2000) 175–178.
- [35] M. Kennedy, B. Runnegar, A. Prave, K. Hoffman, M. Arthur, Two or four Neoproterozoic glaciations?, *Geology* 26 (1998) 1059–1063.
- [36] G. Halverson, A. Maloof, P. Hoffman, The Marinoan glaciation (Neoproterozoic) in northeast Svalbard, *Basin Research* 16 (2004) 297–324.
- [37] M. Edwards, Sedimentology of the Upper Proterozoic glacial record, Vestertana Group, Finnmark, North Norway, *Norges Geologiske Undersøkelse* 384 (1984) 1–76.
- [38] A. Kaufman, A. Knoll, Neoproterozoic variations in the C-isotopic composition of seawater, *Precambrian Research* 73 (1995) 27–49.
- [39] A. Kaufman, A. Knoll, G. Narbonne, Isotopes, ice ages, and terminal Proterozoic Earth history, *Proceedings of the National Academy of Sciences* 95 (1997) 6600–6605.
- [40] J. Higgins, D. Schrag, Aftermath of a snowball Earth, *Geochemistry, Geophysics, Geosystems* 431 (2003) 10.1029/2002GC000403.
- [41] S. Porter, A. Knoll, P. Affaton, Chemostratigraphy of Neoproterozoic cap carbonates from the Volta Basin, West Africa, *Precambrian Research* 139 (2004) 99–112.
- [42] C. Zhou, R. Tucker, S. Xiao, Z. Peng, X. Yuan, Z. Chen, New constraints on the ages of Neoproterozoic glaciations in south China, *Geology* 32 (2004) 337–440.
- [43] Y. Shen, T. Zhang, X. Chu, C-isotopic stratification in a neoproterozoic postglacial ocean, *Precambrian Research* 137 (2005) 243–251.
- [44] P. Hoffman, D. Hawkins, C. Isachsen, S. Bowring, Precise U-Pb zircon ages for early Damaran magmatism in the Summas Mountains and Welwitschia Inlier, northern Damara belt, Namibia, *Communications of the Geological Survey of Namibia* 11 (1996) 47–52.
- [45] B. Goscombe, M. Hand, D. Gray, J. Mawby, The metamorphic architecture of a transpressive orogen: the Kaoko Belt, Namibia, *Journal of*

- Petrology 44 (2003) 679–711.
- [46] H. Porada, V. Berhorst, Towards a new understanding of the Neoproterozoic–early Paleozoic Lufilian and northern Zambezi Belts in Zambia and the Democratic Republic of Congo, *Journal of African Earth Sciences* 30 (2000) 727–771.
  - [47] L. da Silva, N. McNaughton, R. Armstrong, L. Hartmann, I. Fletcher, The neoproterozoic Mantiqueira Province and its African connections: a zircon-based U-Pb geochronologic subdivision for the Brasiliano/Pan-African systems of orogens, *Precambrian Research* 136 (2005) 203–240.
  - [48] K.-H. Hoffmann, A. Prave, A preliminary note on a revised subdivision and regional correlation of the Otavi Group based on glaciogenic diamictites and associated cap dolostones, *Communications of the Geological Survey of Namibia* 11 (1996) 81–86.
  - [49] K.-H. Hoffmann, New aspects of lithostratigraphic subdivision and correlation of late Proterozoic to early Cambrian rock of the southern Damara Belt and their correlation with the central and northern Damara Belt and Gariiep Belt, *Communications of the Geological Survey of Namibia* (1989) 59–67.
  - [50] P. Hoffman, G. Halverson, Otavi Group of the northern platform and the northern margin zone, in: R. M. Miller (Ed.), *Handbook on the Geology of Namibia*, Geological Survey of Namibia, 2005.
  - [51] G. Henry, C. Clendenin, I. Stanistreet, K. Maiden, Multiple detachment model for the early rifting stage of the Late Proterozoic Damara orogen in Namibia, *Geology* 18 (1990) 67–71.
  - [52] H. Porada, H. Ahrendt, H.-J. Behr, K. Weber, The join of the coastal and intracontinental branches of the Damara orogen, Namibia, South West Africa, in: H. Martin, F. Eder (Eds.), *Intracontinental Fold Belts*, Springer-Verlag, 1983, pp. 901–912.
  - [53] G. Halverson, P. Hoffman, D. Schrag, A major perturbation of the carbon cycle before the Ghaub glaciation (Neoproterozoic) in Namibia: prelude to snowball Earth?, *Geochemistry, Geophysics, Geosystems* 3 (2002) 10.1029/2001GC000244.
  - [54] E. Domack, P. Hoffman, Stratigraphic transition into and out of a snowball glacial: evidence from the Otavi platform and Fransfontein slope, Namibia, *EOS Transactions* 84 (46) (2003) C11B–0819.
  - [55] D. C. Frets, Geology and structure of the Huab-Welwitschia area, South West Africa, *Bulletin of Precambrian Research* 5 (1969) 235.
  - [56] P. Hoffman, Carbonates bounding glacial deposits: Evidence for snowball Earth episodes and greenhouse aftermaths in the Neoproterozoic Otavi Group of northern Namibia: Excursion Guide, 16th International Sedimentological Conference, Auckland Park, South Africa, 2002.
  - [57] W. Hegenberger, Gas escape structures in Precambrian peritidal carbonate rocks, *Communications of the Geological Survey of Namibia* 33 (1987) 49–55.
  - [58] P. Hoffman, G. Halverson, J. Grotzinger, Comment: Are Proterozoic cap

- carbonates and isotopic excursions a record of gas hydrate destabilization following Earth's coldest interval? (Kennedy, M.J., Christie-Blick, N., and Sohl, L.E., 2001)., *Geology* 30 (2002) 286–287.
- [59] P. Hoffman, E. Hartz, Large, coherent, submarine landslide associated with Pan-African foreland flexure, *Geology* 27 (1999) 687–690.
- [60] R. Miller, The Owambo basin of Northern Namibia, in: Selley (Ed.), *African Basins*, Elsevier Science, New York, NY, 1997, pp. 237–268.
- [61] M. Kennedy, N. Christie-Blick, L. Sohl, Are Proterozoic cap carbonates and isotopic excursions a record of gas hydrate destabilization following Earth's coldest intervals?, *Geology* 29 (5) (2001) 443–446.
- [62] J. Burdett, M. Arthur, M. Richardson, A Neogene seawater sulfur isotope age curve from calcareous pelagic microfossils, *Earth and Planetary Sciences Letters* 94.
- [63] D. Canfield, R. Raiswell, J. Westrich, C. Reaves, R. Berner, The use of chromium reduction in the analysis of reduced inorganic sulfur in sediments and shales, *Chemical Geology* 54 (1986) 149–155.
- [64] R. Raiswell, D. Canfield, R. Berner, A comparison of iron extraction methods for the determination of degree of pyritisation and the recognition or iron-limited pyrite formation, *Chemical Geology* 111 (1994) 101–110.
- [65] N. Pingitore, G. Meitzner, K. Love, Identification of sulfate in natural carbonates by x-ray absorption spectroscopy, *Geochimica et Cosmochimica Acta* 59 (12) (1995) 2477–2483.
- [66] A. Kampschulte, H. Strauss, The sulfur isotopic evolution of Phanerozoic seawater based on the analysis of structurally substituted sulfate in carbonates, *Chemical Geology* 204 (2004) 255–286.
- [67] W. Staudt, M. Schoonen, Sulfate incorporation into sedimentary carbonates, in: M. Vairavamurthy, M. Schoonen (Eds.), *Geochemical transformations of sedimentary sulfur*, American Chemical Society, Washington, D.C., 1995, pp. 332–345.
- [68] J. Erez, The source of ions for biomineralization in foraminifera and their implications for paleoceanographic proxies, in: P. Dove, J. DeYoreo, S. Weiner (Eds.), *Biomineralization*, Mineralogical Society of America, Washington, D.C., 2003, pp. 115–149.
- [69] P. Baker, M. Kastner, Constraints on the formation of sedimentary dolomite, *Science* 213.
- [70] S. Kasemann, C. Hawkesworth, A. Prave, A. Fallick, P. Pearson, Boron and calcium isotope composition in Neoproterozoic carbonate rocks from Namibia: evidence for extreme environmental change, *Earth and Planetary Science Letters* 231 (2005) 73–86.
- [71] L. Land, The isotopic and trace element geochemistry of dolomite: the state of the art, in: D. Zenger, J. Dunham, R. Ethington (Eds.), *Concepts and Models of Dolomitization*, SEPM, Tulsa, 1980, pp. 87–111.
- [72] W. Hyde, T. Crowley, S. Baum, W. Peltier, Neoproterozoic 'snowball Earth' simulations with a coupled climate/ice-sheet model, *Nature* 405

- (2000) 425–429.
- [73] G. Jiang, M. Kennedy, N. Christie-Blick, Stable isotopic evidence for methane seeps in Neoproterozoic postglacial cap carbonates, *Nature* 426 (2003) 822–826.
- [74] K. Habicht, M. Gade, B. Thamdrup, P. Berg, D. Canfield, Calibration of sulfate levels in the Archean ocean, *Science* 298 (2002) 2372–2374.
- [75] B. Bodiselitsch, C. Koeberl, S. Master, W. Reimold, Estimating duration and intensity of Neoproterozoic snowball glaciations from Ir anomalies, *Science* 308 (2005) 239–242.
- [76] C. Vasconcelos, J. McKenzie, S. Bernasconi, D. Grujic, A. Tien, Microbial mediation as a possible mechanism for natural dolomite formation at low temperatures, *Nature* 377 (1995) 220–222.
- [77] S. Sheppard, H. Schwarz, Fractionation of carbon and oxygen isotopes and magnesium between coexisting metamorphic calcite and dolomite, *Contributions to Mineralogy and Petrology* 26 (1970) 161–198.
- [78] B. Lewis, W. Landing, The biogeochemistry of manganese and iron in the Black Sea, *Deep-Sea Research* 38 (1991) S773–803.
- [79] P. V. Cappellen, E. Viollier, A. Roychoudhury, L. Clark, E. Ingall, K. Lowe, T. Dichristina, Biogeochemical cycles of manganese and iron at the oxic-anoxic transition of a stratified marine basin (orca basin, gulf of mexico), *Environmental Science and Technology* 32 (1998) 2931–2939.
- [80] M. Hurtgen, T. Lyons, E. Ingall, A. Cruse, Anomalous enrichment of iron monosulfide in euxinic marine sediments and the role of H<sub>2</sub>S in iron sulfide transformations: examples from Effingham Inlet, Orca Basin, and the Black Sea, *American Journal of Science* 299 (1999) 556–588.
- [81] J. Wijsman, J. Middleburg, C. Heip, Reactive iron in Black Sea sediments: implications for iron cycling, *Marine Geology* 172 (2001) 167–180.
- [82] B. Jørgenson, D. Nelson, Sulfide oxidation in marine sediments: geochemistry meets microbiology, in: J. Amend, K. Edwards, T. Lyons (Eds.), *Sulfur Biogeochemistry—Past and Present: Geological Society of America Special Paper 379*, 2004, pp. 63–81.
- [83] Y. Shen, A. Knoll, M. Walter, Evidence for low sulphate and anoxia in a mid-proterozoic marine basin, *Nature* 423 (2003) 632–635.
- [84] T. Goldberg, S. Poulton, H. Strauss, Sulphur and oxygen isotope signatures of late Neoproterozoic to early Cambrian sulphate, Yangtze Platform, China: Diagenetic constraints and seawater evolution, *Precambrian Research* 137 (2005) 223–241.